

DARK CURRENT AND PHOTOCURRENT ANALYSIS OF PLASMONIC  
NANO-ANTENNA PHOTODETECTOR

BY

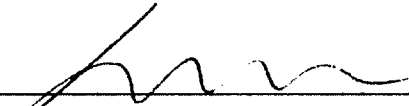
THITIKORN KEMSRI  
B.S. ROYAL THAI NAVAL ACADEMY (2011)

SUBMITTED IN PARTIAL FULFILLMENT OF THE REQUIREMENTS  
FOR THE DEGREE OF MASTER OF SCIENCE  
DEPARTMENT OF ELECTRICAL AND COMPUTER ENGINEERING  
UNIVERSITY OF MASSACHUSETTS LOWELL

Signature of

Author:  Date: 11/12/15

Signature of Thesis

Supervisor:  11/17/15

Name Typed: Professor Xuejun Lu

Signatures of Other Thesis Committee Members:

Committee Member Signature: 

Name Typed: Professor Kavitha Chandra

Committee Member Signature: 

Name Typed: Professor Wei Guo

Committee Member Signature: 

Name Typed: Professor Guiru Gu

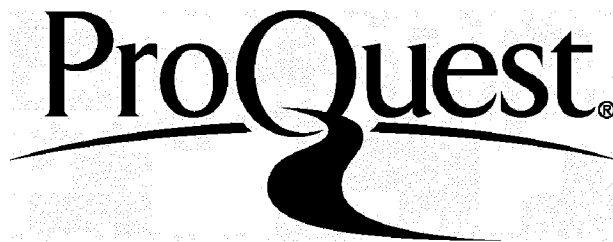
ProQuest Number: 10003305

All rights reserved

INFORMATION TO ALL USERS

The quality of this reproduction is dependent upon the quality of the copy submitted.

In the unlikely event that the author did not send a complete manuscript and there are missing pages, these will be noted. Also, if material had to be removed, a note will indicate the deletion.



ProQuest 10003305

Published by ProQuest LLC(2016). Copyright of the Dissertation is held by the Author.

All rights reserved.

This work is protected against unauthorized copying under Title 17, United States Code.  
Microform Edition © ProQuest LLC.

ProQuest LLC  
789 East Eisenhower Parkway  
P.O. Box 1346  
Ann Arbor, MI 48106-1346

**DARK CURRENT AND PHOTOCURRENT ANALYSIS OF  
PLASMONIC NANO-ANTENNA PHOTODETECTOR**

**BY**

**THITIKORN KEMSRI**

**ABSTRACT OF A THESIS SUBMITTED TO THE FACULTY OF THE  
DEPARTMENT OF ELECTRICAL AND COMPUTER ENGINEERING  
IN PARTIAL FULFILLMENT OF THE REQUIREMENTS  
FOR THE DEGREE OF  
MASTER OF SCIENCE  
UNIVERSITY OF MASSACHUSETTS LOWELL**

**2015**

**Thesis Supervisor: Xuejun Lu, Ph.D,**

**Professor, Department of Electrical and Computer Engineering.**

## **ABSTRACT**

Surface plasmonic resonance (SPR) plays important roles in performance enhancement in the Quantum Dot Infrared Photodetector. It can increase the photoresponse, SPR induced surface confinement and electromagnetic field enhancement. The angular dependence of the SPR enhancement effect has been fully investigated. In this thesis, the angular dependent effects of the two dimensional subwavelength hole array (2DSHA) and circular disk array (CDA) plasmonic structures are analyzed and compared with regular quantum dot photodetector. The photocurrent and dark current of both SPR structures are at different angles. The CDA plasmonic structure shows stronger angular dependence pattern than the 2DSHA plasmonic structure. The angular dependence is analyzed and agrees with the radiation pattern of a circular aperture antenna.

## **ACKNOWLEDGMENT**

During the time of my study life, I would like to thank you my supervisor, Prof. Xuejun Lu, who allows me the best opportunities to conduct the research in the greatest topic and his patience. Without support and advice from my supervisor, I could not finish my research and understand all of sophisticated contents.

I also appreciate my warm family and friends with my wholeheartedness to encourage me and dedicate their time during the study time.

Furthermore, I would like to thank the committees, Prof. Wei Guo, Prof. Guiru Gu, and Prof. Kavitha Chandra for their efforts to review my thesis and their useful comments.

# TABLE OF CONTENTS

<u>I.</u>	INTRODUCTION.....	1
1.1	Principle of Photodetector.....	1
1.2	IR Radiation and Wavelength.....	3
1.3	IR Applications.....	4
1.4	Characteristics of IR Photodetector.....	5
1.4.1	Quantum Well Infrared Photodetector.....	6
1.4.2	Quantum Dot Infrared Photodetector.....	7
1.5	Background of Plasmonic structure.....	10
1.6	Pattern of Surface Plasmon.....	12
<u>II.</u>	FABRICATION.....	16
2.1	Concept and Fabrication.....	16
2.2	Fabrication Process.....	16
2.2.1	QDIP Fabrication Procedure.....	17
2.2.2	Plasmonic Fabrication Procedure.....	21
2.3	Atomic Force Microscopy.....	25
<u>III.</u>	DARK CURRENT AND PHOTOCURRENT ANALYSIS.....	28
3.1	Dark Current Test Set Up.....	28
3.2	Dark Current's Experimental Results.....	30

3.3	Photocurrent Test Set Up.....	34
3.4	Photocurrent's Experimental Results.....	36
3.5	The measurement at different angle.....	37
<u>IV.</u>	CONCLUSION.....	52
<u>V.</u>	FUTURE WORK.....	54

## LIST OF ILLUSTRATIONS

Figure 1.1 Discrete Set of Energy Level.....	1
Figure 1.2 The basic principle of semiconductor.....	2
Figure 1.3 Electromagnetic wavelength.....	3
Figure 1.4 Infrared Night Vision Goggle .....	4
Figure 1.5 Brief reviews in Electron Hole Pairs.....	5
Figure 1.6 The ideal model of QWIPs with the direction how the growth goes and the well barrier to trap the electron .....	7
Figure 1.7 The ideal structure of QDIPs that is different from QWIPs at the rectangular barrier .....	8
Figure 1.8 The basic principle of the QWIPs and QDIPs .....	9
Figure 1.9 a. A replica of Lycurgus cup in the day time b. light transmission through the cup .....	10
Figure 1.10 a. The circular pattern and b. the regular pattern on MTM.....	13
Figure 1.11 a. The metallic stripe on the surface and b. The absorption with different angles from incident light .....	13
Figure 1.12 a. The size of 2dimension-hole arrays and b. The spectrum of hole can confine the electromagnetic field.....	14
Figure 1.13 Dot arrays or circular disc structure .....	15
Figure 1.14 a. The circular disc structure and b. The absorption profile.....	15
Figure 2.1 QDIP Fabrication Procedure.....	17



Figure 2.2 QDIP Fabrication Procedure .....	17
Figure 2.3 QDIP Fabrication Procedure .....	18
Figure 2.4 QDIP Fabrication Procedure .....	18
Figure 2.5 QDIP Fabrication Procedure.....	18
Figure 2.6 QDIP Fabrication Procedure.....	18
Figure 2.7 QDIP Fabrication Procedure.....	19
Figure 2.8 QDIP Fabrication Procedure .....	19
Figure 2.9 QDIP Fabrication Procedure .....	19
Figure 2.10 QDIP Fabrication Procedure.....	19
Figure 2.11 The plasmonic structure of 2DSHA .....	20
Figure 2.12 The plasmonic structure of Dot Arrays .....	21
Figure 2.13 Plasmonic Fabrication Procedure .....	21
Figure 2.14 Plasmonic Fabrication Procedure .....	21
Figure 2.15 Plasmonic Fabrication Procedure .....	22
Figure 2.16 Plasmonic Fabrication Procedure .....	22
Figure 2.17 Plasmonic Fabrication Procedure .....	22
Figure 2.18 Plasmonic Fabrication Procedure .....	22
Figure 2.19 Plasmonic Fabrication Procedure .....	23
Figure 2.20 Plasmonic Fabrication Procedure .....	23
Figure 2.21 Plasmonic Fabrication Procedure .....	23
Figure 2.22 Plasmonic Fabrication Procedure .....	23

Figure 2.23 a. The regular structure with top electrode and bottom electrode, b. The top of mesa has been aligned with 2D SHA, c. The structure of SP, d. Diameter of the 2D SHA mask.....	24
Figure 2.24 The sample has mounted on the copper plate and bounded with the wire.....	24
Figure 2.25 How the AFM works.....	24
Figure 2.26 a. AFM amplitude image (2 $\mu\text{m}$ ×2 $\mu\text{m}$ ) and b. The image size 1 $\mu\text{m}$ ×1 $\mu\text{m}$ .....	26
Figure 2.27 a. Topography image (2 $\mu\text{m}$ ×2 $\mu\text{m}$ ) and b. The image size 1 $\mu\text{m}$ ×1 $\mu\text{m}$ .....	27
Figure 3.1 The setup of the dark current without aluminum shield .....	29
Figure 3.2 The setup of the dark current with aluminum shield.....	29
Figure 3.3 The dark current density for dot arrays at port 1 (mesa1) with and without aluminum shield.....	30
Figure 3.4 The dark current density for reference at port 1 (mesa1) with and without aluminum shield.....	31
Figure 3.5 The dark current density for hole arrays at port 1 (mesa1) with and without aluminum shield.....	32
Figure 3.6 Percentage of Dark Current Enhancement.....	33
Figure 3.7 The photocurrent measurement without aluminum shield .....	35
Figure 3.8 The photocurrent measurement with aluminum shield .....	35
Figure 3.9 The angles testing for the photocurrent .....	37

Figure 3.10 Measurement at 0 degree.....	38
Figure 3.11 Measurement at 0 degree .....	38
Figure 3.12 Measurement at 0 degree .....	39
Figure 3.13 Measurement at 30 degree .....	40
Figure 3.14 Measurement at 30 degree .....	40
Figure 3.15 Measurement at 30 degree.....	41
Figure 3.16 Measurement at 45 degree .....	42
Figure 3.17 Measurement at 45 degree .....	42
Figure 3.18 Measurement at 45 degree .....	43
Figure 3.19 Measurement at 60 degree .....	44
Figure 3.20 Measurement at 60 degree.....	44
Figure 3.21 Measurement at 60 degree .....	45
Figure 3.22 The ratio of the dot arrays over the references.....	48
Figure 3.23 The ratio of the hole arrays over the references .....	49
Figure 3.24 the three- dimensional field of the circular aperture.....	51

## **LIST OF TABLES**

Table 1.1 The photocurrent at different angles .....	46
Table 1.2 The photocurrent of the dot arrays over reference in different angles.....	47
Table 1.3 The photocurrent of the hole arrays over reference in different angles....	50

# **I. INTRODUCTION**

## **1.1 Principle of Photodetector**

Photodetectors are opto-electronic devices that convert light signals to electrical signals. Depending on the detection wavelengths, detectors can be made in various materials such as InGaAs, InGaP, InAs and GaAs substrates. By collecting photoexcited electrons from the discrete set of energy levels of detector materials, one can obtain photocurrent.

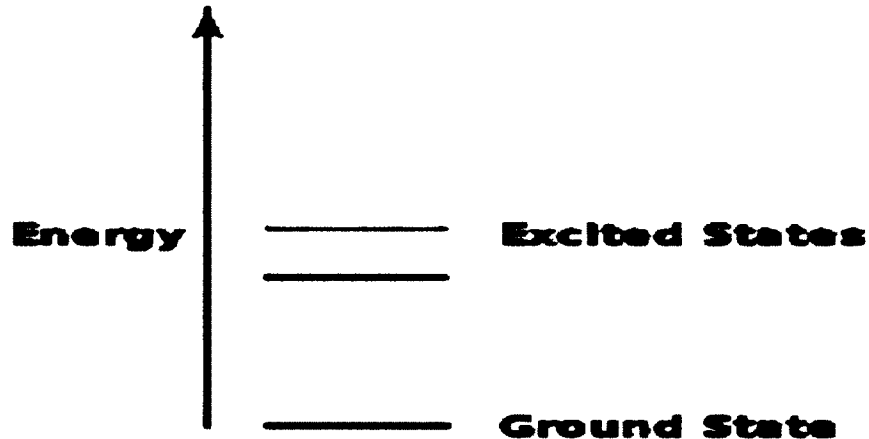


Figure 1.1 Discrete Set of Energy Level.

*\*Image from [https://en.wikipedia.org/wiki/Energy\\_level](https://en.wikipedia.org/wiki/Energy_level)*

To physically create the free electron, it can be described by the energy of electron. When the electrons have the sufficient energy by adding the energy, it can

transit from the valence band passing through the band gap (ground state) to conducting band (upper state).

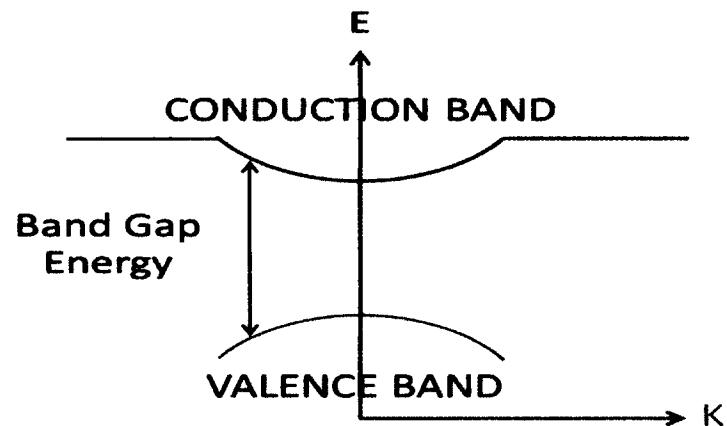


Figure 1.2 the basic principle of semi-conductor.

The energy has to be greater than or equal to the energy gap of material.

Otherwise, the electrons are not able to move to the upper state.

The formula is

$$E = h\nu = \frac{hc}{\lambda} \quad \{1\}$$

E: Photon's energy

h: Planck's constant

c: Speed of light

$\nu$ : Frequency of light

$\lambda$ : Wavelength

## 1.2 Infrared (IR) Radiation and Wavelength

In a few years, there are many researchers focusing on performance of the infrared and the visible light. Especially, infrared light has plenty of advantages in sections of wavelength between the 0.78 -1000  $\mu\text{m}$ .

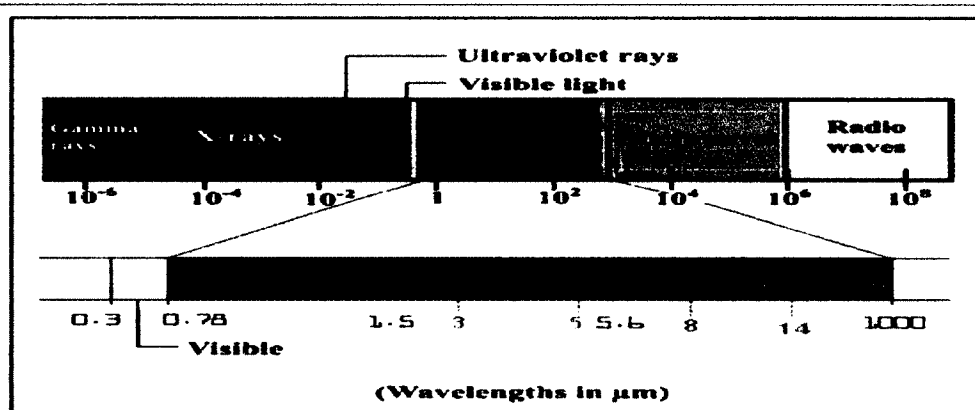


Figure 1.3 Electromagnetic wavelength.

*\*Image from <http://www.eluox.com/en/Thermograph>*

The Short-wave infrared is (SWIR) around 0.78-1.0  $\mu\text{m}$ . The Mid-wave infrared (MWIR) is from 1.0 to 3.0  $\mu\text{m}$  and the long-wave infrared (LWIR) covers from 8-12  $\mu\text{m}$ . Human eyes are not able to see the infrared light but the object can be detected with appropriate temperature. The photodetector is the one that plays an important role in several industries since the performance of this device, responsitivity, quantum efficiency, detectivity, have been used for a variety of commercial applications such as infrared cameras, infrared weapons, and sensors.

### 1.3 Infrared Applications

In the field of infrared development, many devices have been improved to take the benefits of infrared wavelength in the industrial field, medical or surgery [1] and also military as the remote sensor device, which is detection and identification of enemy in the darkness as the sensor receive the radiation that is reflected by the target [2].

Figure 1.4 illustrates the man in the field can be detected by IR sensors of Army military in the night to identify whether man is friend or foe.

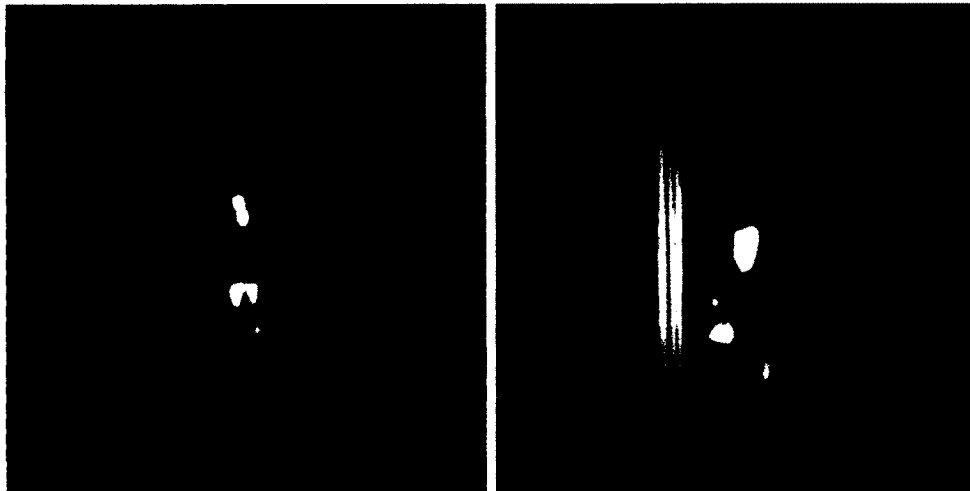


Figure 1.4 Infrared Night Vision Goggle.

*\*Image from /www.photonics.com*



#### 1.4 Characteristics of Infrared Photodetector

Generally, the infrared photodetector is about the process to change the light or electromagnetic wave to the electrical current in the infrared spectral regions. For example, in the interband transition photodetector, the light is photon. When they absorb the energy that is more than or equal to the band gap of material, they will produce the electron hole pair (EHP) between the conduction band and the valence band and then generate the photocurrent. However, the type of infrared photodetector will be widely described by interband transition photodetector and intersubband transition photodetector.

##### Interband Transition photodetector

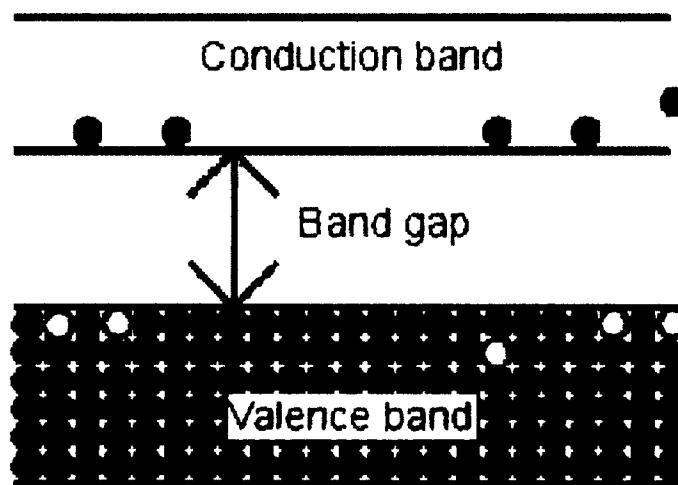


Figure 1.5 Brief reviews in Electron Hole Pair.

*\*Image from <http://www.rpi.edu/dept/phys/ScIT/InformationProcessing/semicond>*

The brief review is explained by the energy level from the bottom band (valence band) to the upper band (conduction band). The incident photon with sufficient energy rising to the conduction band generates the electron hole pair (EHP) with electric field surrounding the device. Then it is measured by electrode and forms the photocurrent.

#### Intersubband Transition Photodetector

This photodetector is manufactured by Molecular Beam Epitaxy (MBE) with a number of layers of different materials and create the energy levels within conduction band to valence band by controlling the thickness. The area of research in the intersubband transition photodetector consists of Quantum Well Infrared Photodetector (QWIP) [3] and Quantum Dot Infrared Photodetector (QDIP).

##### **1.4.1 Quantum Well Infrared Photodetector**

For the quantum well infrared photodetector, the structure has 2 dimensional confinements, which is composed of conduction band and valence band. Examples of the quantum well, Bulk semiconductor [4] and Multi-quantum well layers [5], which are two bulk semiconductors combining together (semiconductor heterostructure).

Also, the structure of the quantum well photodetector is different from the quantum dot photodetector at the well barrier as the ideal model following [6].

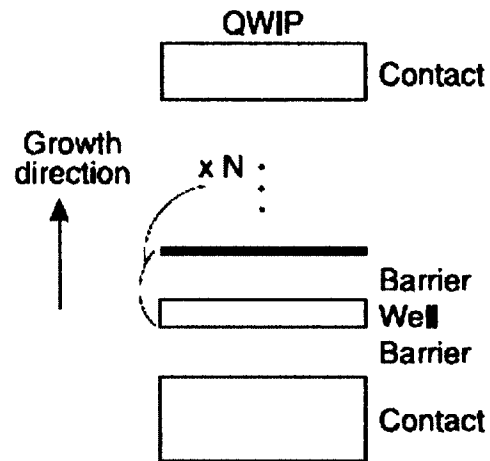


Figure 1.6 shows the ideal model of QWIPs with the direction how the growth goes and the well barrier to trap the electron [6].

*\*Image from Quantum dot infrared photodetector, Opto-electronics review,*

*Author: H.C. LIU*

Moreover, there are many advantages of quantum well. First it is the quality of imaging application when comparing with HgCdTe detector [7] (HgCdTe is the state-of-art in the interband transition photodetector that has plenty of enhancement and wide range of SWIR, MWIR, and LWIR). Secondly, it is not difficult for fabrication. Lastly, it is lower in cost than other infrared detectors.

#### 1.4.2 Quantum Dot Infrared Detector

The structure of quantum dot infrared detector has 3 dimensional confinements. In general, the principle is similar to the QWIPs, converting light to

electrical signal, which is the light radiating the surface of the detector and then the electron moving from the ground state to excited state. The electron will move through the potential barrier when the device is applied by bias voltage and converted to photocurrent. The ideal model of the quantum dot infrared detector is

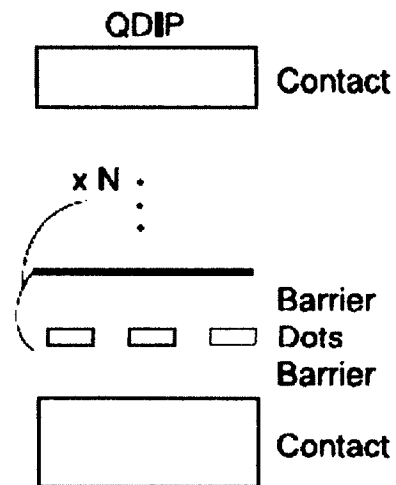


Figure 1.7 shows the ideal structure of QDIPs that is different from QWIPs at the rectangular barrier [6].

*\*Image from Quantum dot infrared photodetector, Opto-electronics review, Author:*

*H.C. LIU*

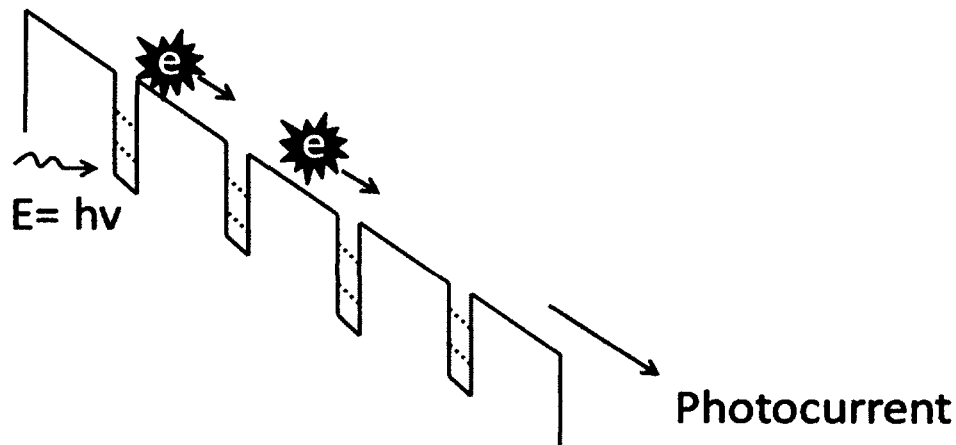


Figure 1.8 demonstrates the basic principle of the QWIPs and QDIPs.

Even though the quantum well (QWIPs) have several advantages, the QDIPs also are better than QWIPs. First, the QDIP has longer excited life time. Second, it has lower dark current than QWIP which has density of states (DOS) much more than QDIP. The last is the higher responsivity and detectivity.

For the overview, to design and control the performance of the devices, it has to be concerned with the characteristic of the material. Therefore, in the next chapter, we will discuss the fabrication process and what the growth should be in order to achieve the qualities of infrared photodetector with low dark current and strong sensitivity.

### 1.5 Background of Plasmonic Structure

Surface Plasmon (SP) or Plasmonic structures have been published in several journals. Especially, in the optical commercials the plasmonic structure has 3 advantage. First, with its structure it has enhancement of the field since the surface of the plasmon results in the resonant cavity to improve the electromagnetic field. Second, the plasmonic layer that is deposited on the surface help the most of incident light trapped into the area of the device due to this structure can use the ability of metal-dielectric interface. Third, the plasmonic structure has several performances such as the photo response, the conductivity, the low noise current.

Based on the near- field effect, the plasmonic feature leads to the free electron passing through the surface with electromagnetic wave (light). In general, the metal media has the different shape, size, and also the material such as the thin film. That brings about the resonance within the surface area. The fundamental example is Lycurgus Cup or a roman technology [10].

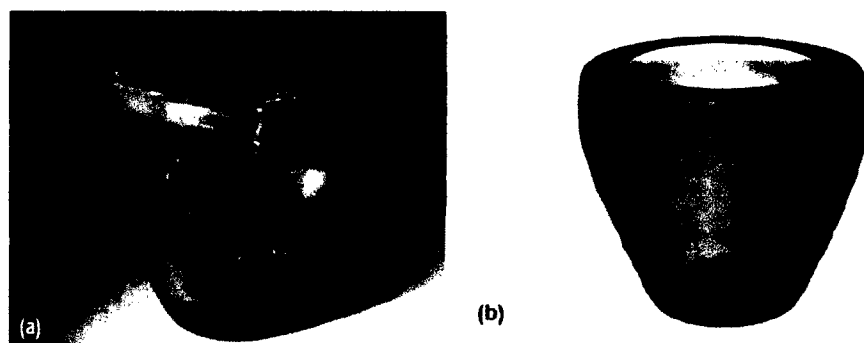


Figure 1.9 a. A replica of Lycurgus cup in the day time b. light transmission through the cup [10].

According to the figure 1.9 above, the changes of color depend on the angle of the illumination. For example, in the noon time the cup is green when the cup is reflected by the light. On a contrary, the cup is red when the light is passing through the glass because this ancient cup has the ratio of gold and silver within the glass in appropriate portions. With the sophisticated properties, many applications and development have been researched. The localized surface plasmon, which is the oscillation of free electrons within the glass passing the metallic particles, has been modeled by Richie [11]. This contributes to the resonance frequency and the propagation of the surface electromagnetic wave around the surface area or the metal-dielectric interface [12].

The theory to understand the plasmonic structure with excitation-effect focuses on the local surface plasmon which has the following formula [9]:

$$\alpha = 4\pi a^3 \frac{\epsilon_m - \epsilon_d}{\epsilon_m + 2\epsilon_d} \quad \{2\}$$

where  $a$  is the radius of the particles,

$\epsilon_d$  is the dielectric constant of the medium,

$\epsilon_m$  is the dielectric constant of metal, and

$\alpha$  is the polarization

The purpose is to increase the polarization on the surface as much as possible in order to rise up the resonance frequency. Also the polarization ( $\alpha$ ) can be the maximum as

the dielectric for the medium matches the dielectric of the metal. Another theory is the surface polaritons which is the transmission of the electromagnetic wave or K wave direction of surface plasmon. The formula that can describe the phenomena of the surface plasmon along the boundary condition of Helmholtz equation [14, 15]:

$$k_{SPP} = k_0 \sqrt{\frac{\epsilon_m \epsilon_d}{\epsilon_m + \epsilon_d}} \quad \{3\}$$

$k_{SPP}$  : the wave vector of surface plasmons,

$k_0$  : the wave vector in free space

## 1.6 Patterns of the Surface Plasmon

With the characteristics of the plasmonic structure, several patterns have been designed in order to increase the electric field and light absorption. The geometries, such the circular disc [18] or dots array, rectangular patterns[17] have been used in the commercials and also in the military within the broad band and dual band such as the mid and the long wavelength infrared. However, to invent the devices with abilities of absorption and high electric field depends on the shape, the size, and the medium interacting between the metal and dielectric. For instance, the reduction of the geometry has processed into the nano-particles at the optical regions. It improves the absorption in wide range (figure 2.3 and 2.4).





Figure 1.10a the circular pattern [18] and Figure 1.10b the regular pattern on MTM [17].

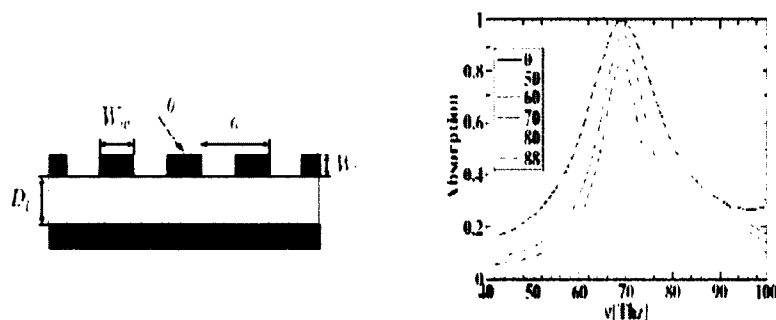


Figure 1.11, Illustrate the metallic stripe on the surface and Figure 1.11b the absorption with different angles from incident light [19].

Such arrays of the rectangular leads to the perfect absorption by tuning the size. That gives to the resonance within full width of half maximum power (FWHM) [21]. Although adjusting the size and the shapes is significant, the type of the material is also essential to consider for the surface plasmon. The gold is responsible for the conductivity and reflection since the gold generally has these characteristics at low frequency but when the incident light pass through, the ability occurs in the high

frequency. That contributes to the surface plasmon resonance with free electron interacting the metal and the dielectric.

The previous works in our group research, one is the hole- arrays pattern with 2 dimensions, was fabricated and studied [8, 9].

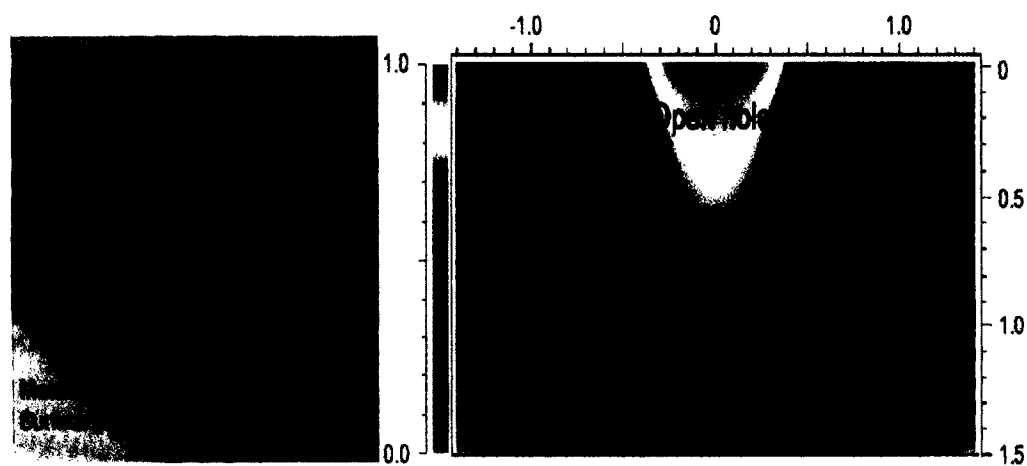


Figure 1.12, (a) the size of 2dimension of hole arrays; (b). the spectrum of hole can confine the electromagnetic filed (from [8, 9]).

From the picture above, the 2DSHA structure have the advantages such as low loss, high conductivity, light confinement in the hole arrays with diameter 1.2  $\mu\text{m}$ , and tunable the functionality. Another design is the dot arrays structure.

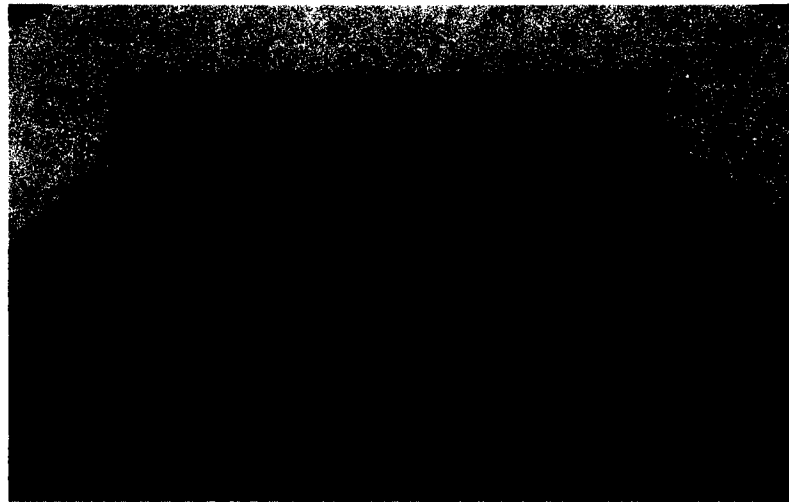


Figure 1.13, Dot arrays or circular disc structure.

For instance, the circular disc [20] in metamaterial on the surface plasmon. The circular shape has different periodicity in vertical and horizontal. Also the diameter is not equal to the other particles. However, with its characteristic still affects more polarization and electromagnetic field including more absorption on the surface of the device (Figure2.6).

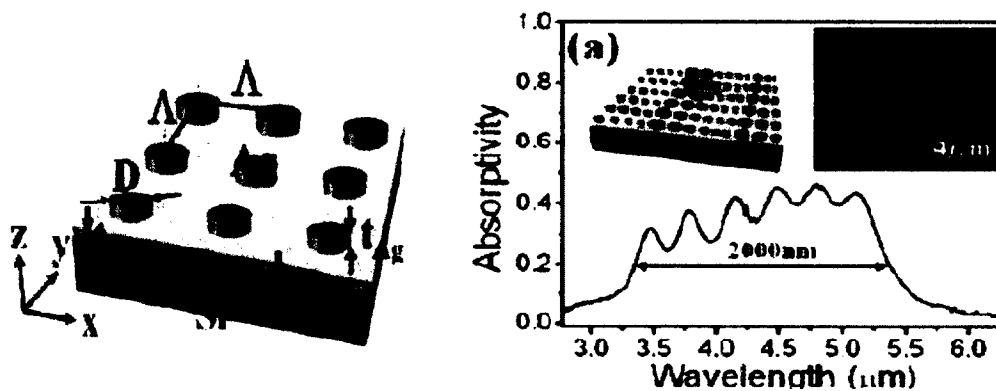


Figure 1.14, (a) the circular disc structure; (b) the absorption profile (from [20]).

## **II. FABRICATION**

### **2.1 Concept and Fabrication Process**

To get the data and evaluate the result, we have to start from the material (wafer) to grow by MBE with Quantum Dots 10 layers within GaAs substrate. MBE is a growth process by molecule beam epitaxial to grow layer by layers with appropriate temperature. Then we use the sample that it stems from MBE to produce the devices. Such as making the electrode on sample for test or fabricating the pattern on sample. Finally, the sample becomes the device and it is ready to test and analyze the performances.

### **2.2 Fabrication Process**

After the sample is grown, the sample will be ready for the fabrication. We will begin the first step (Figure 2.1). The sample needs to be cleaned with Acetone and Isopropanol within Ultrasonic Cleaner for 2 minutes each of the Acetone and Isopropanol. When it is completely cleaned, the sample will be coated with the photoresist (Figure 2.2) and the Lithography process which is shining light on the Mask (Figure 2.3) with the pattern of Quantum dots 4 by 4 arrays for the bottom layer (Figure 2.4). Then the sample is exposed with the pattern on the top and developed by MA-26 for 1 minute. Also the sample has to be etched to the contact layer by  $2\text{H}_2\text{SO}_4 + 16\text{H}_2\text{O}_2 + 160\text{H}_2\text{O}$  (Figure 2.5). Now, the sample is reached to the contact layer for electrode device. The lithography process (Figure 2.7) will take place again with another pattern for the top layer and developed again with MA-26 for 1 minute

(Figure 2.8) after coating the photoresist (Figure 2.6). And then, the next step is the metal deposition (Figure 2.9) to deposit Ni, Ge, Au, Ni and Au on the top of mesa (50Å, 170 Å, 330Å, 150Å, and 3000Å). After finishing the metal deposition, the process is lift-off which is making the sample with the pattern as we desired (Figure 2.10). It is about putting the sample into the cup of acetone within the ultrasonic cleaner until the structure comes up and clearly to see the feature on the surface. Finally, the annealing process is last thing to consider and make the device completely with good feature.

### 2.2.1 QDIP Fabrication Procedure

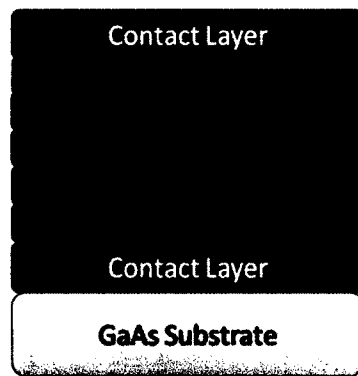


Figure 2.1

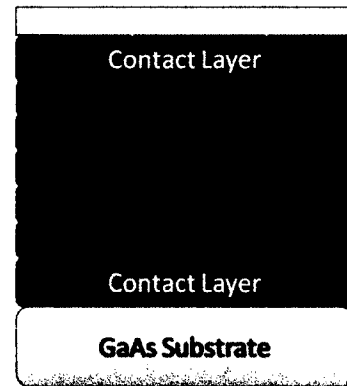


Figure 2.2

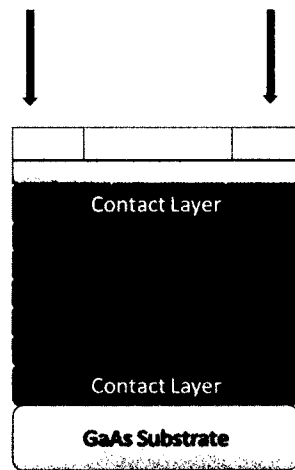


Figure 2.3

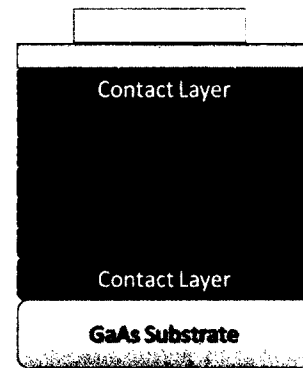


Figure 2.4

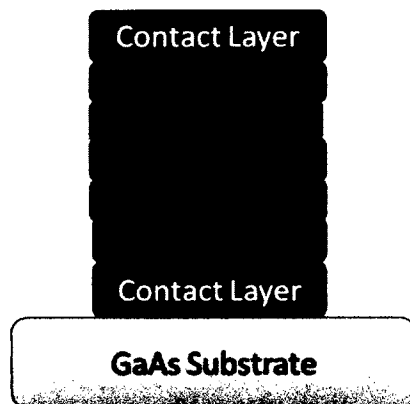


Figure 2.5

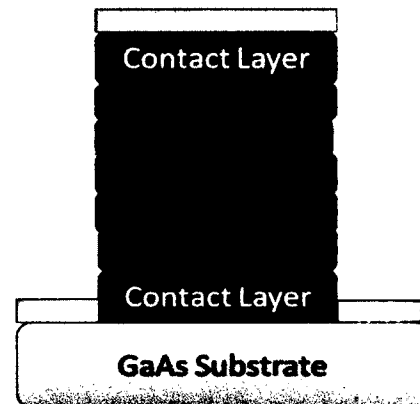


Figure 2.6

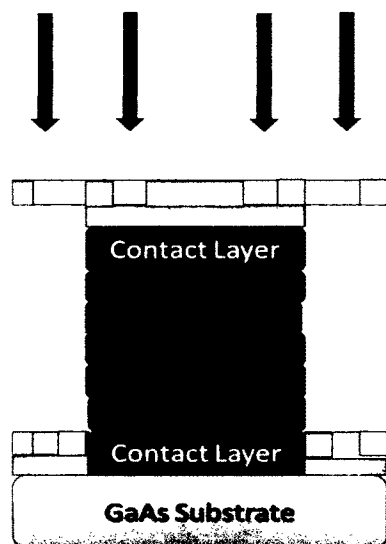


Figure 2.7

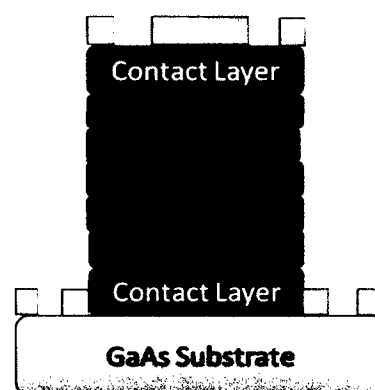


Figure 2.8

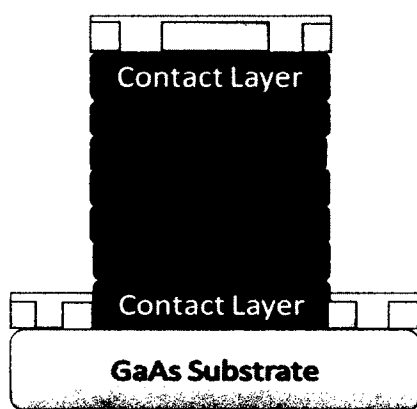


Figure 2.9

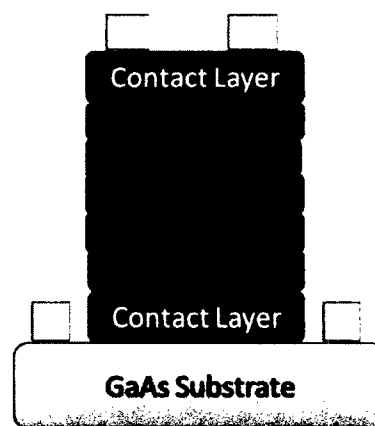


Figure 2.10

### Fabrication of Plasmonic Structure

The plasmonic structure has been processed by the E-beam lithography that emit precisely the electron on the surface of substrate to create the tiny structure with high-resolution, well-quality, and without destroying through the substrate [8]. After the e-beam lithography process has been finished, the surface of the sample has the feature as the figure below. Then, the fabrication process has initialed as the same as the regular fabrication procedure such the figure below.

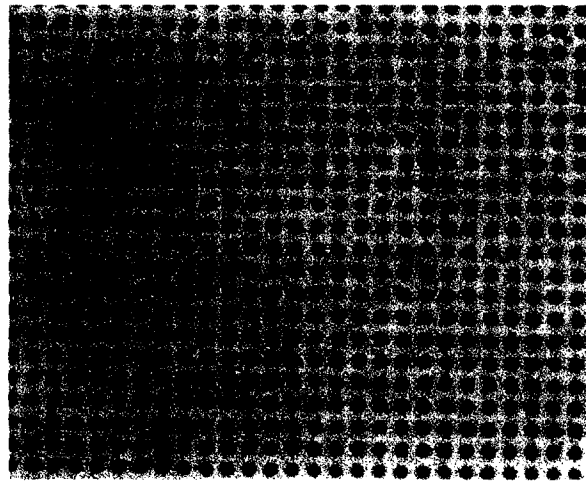


Figure 2.11 the plasmonic structure of 2D SHA[8].





Figure 2.12 the plasmonic structure of Dot Arrays.

#### Plasmonic Fabrication Procedure

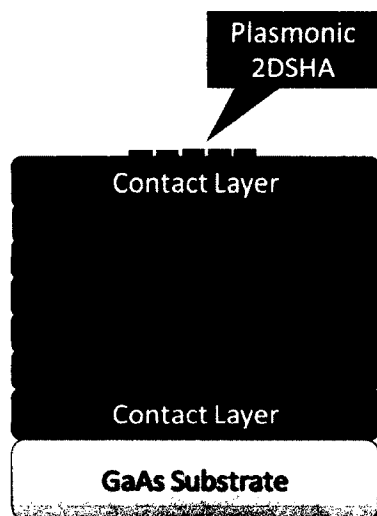


Figure 2.13

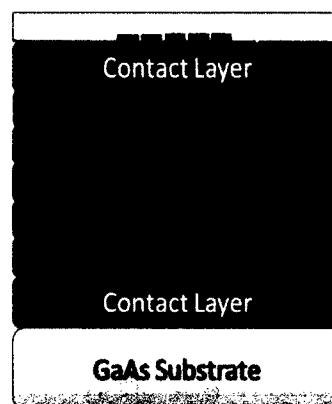


Figure 2.14

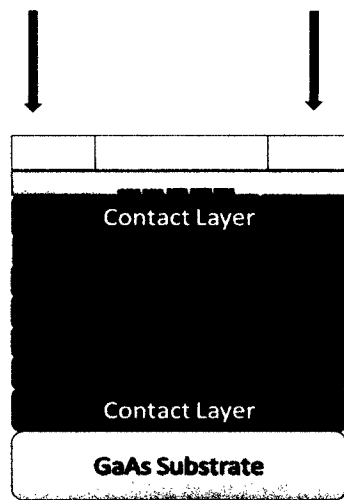


Figure 2.15

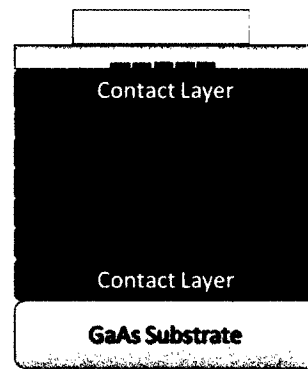


Figure 2.16

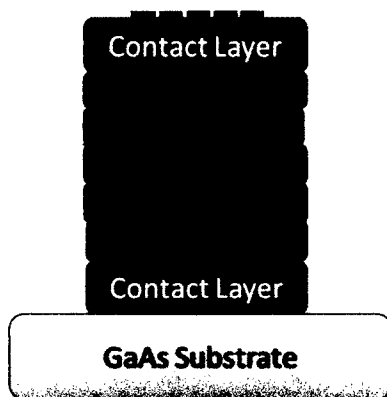


Figure 2.17

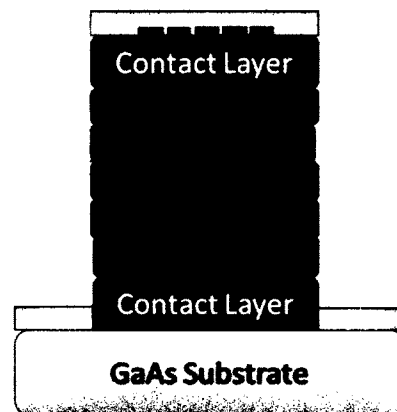


Figure 2.18

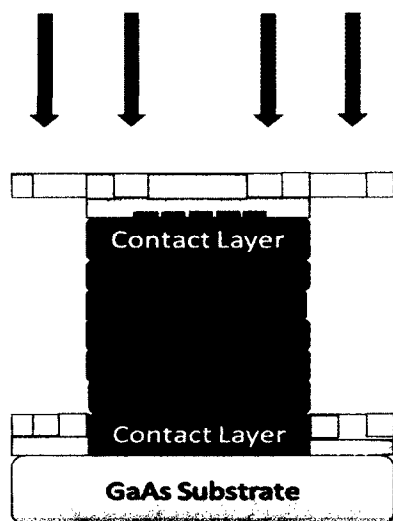


Figure 2.19

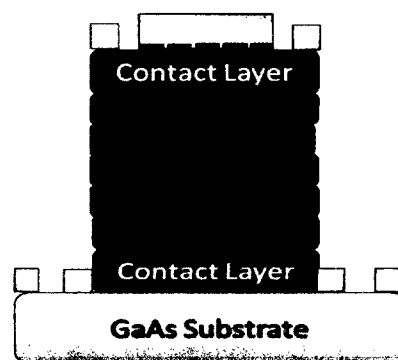


Figure 2.20

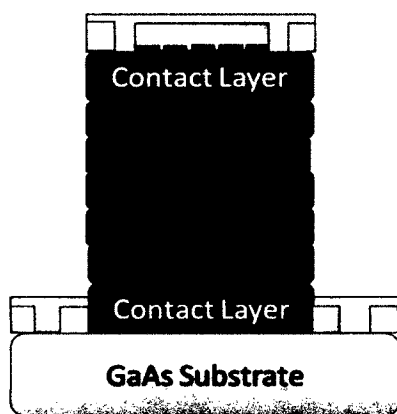


Figure 2.21

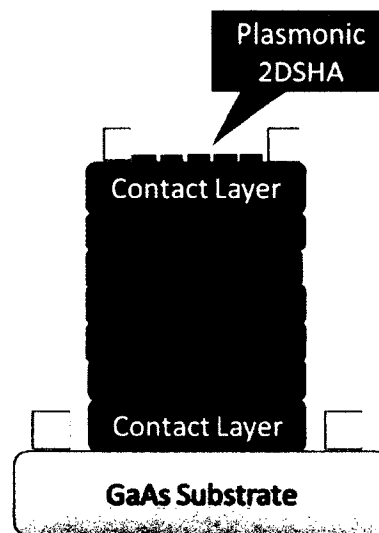


Figure 2.22

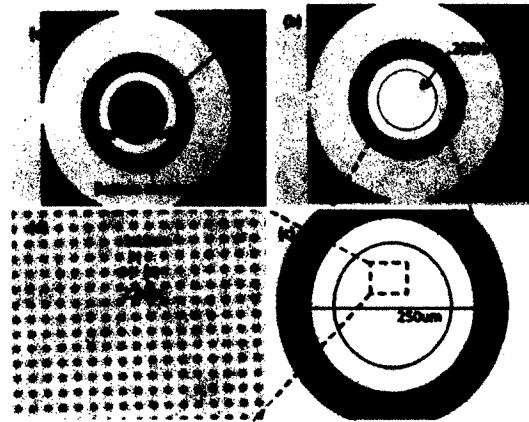


Figure 2.23 [8] a. the regular structure with top electrode

And bottom electrode, b. the top of mesa had been aligned with

2DSHA, c. magnified the structure of SP, d. diameter of the 2DSHA mask.

Finally, the sample is attached on the copper plate and bounded with wire at the circular in each of mesa. Now, the sample is ready for measurement (figure 2.23).

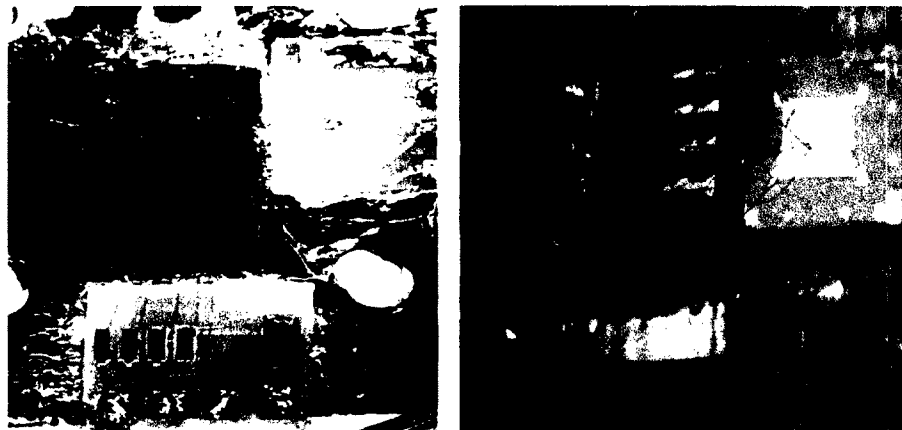


Figure 2.24, the sample is mounted on the copper plate and bounded with the wire [9].

### 2.3 Atomic Force Microscopy

AFM or atomic force microscopy, which is the measurement of the very small features on the surface of the sample, was developed later after STM (Scanning Tunneling Microscopy) was invented by Gerd Binnig and Heinrich Rohrer [16].

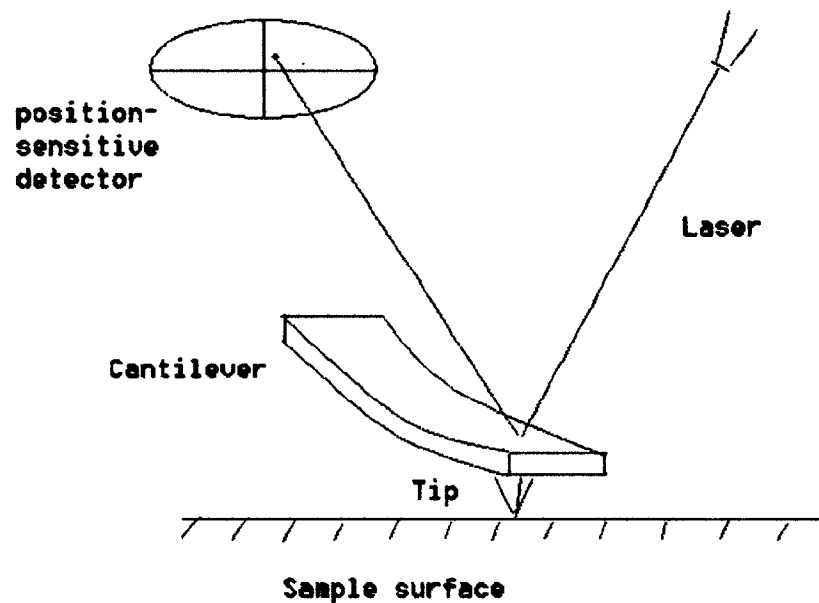


Figure 2.25 How the AFM works.

*Image from <http://www.nanoscience.gatech.edu/zlwang/research/afm.html>*

STM is the fundamental equipment to get the images of nanoparticles on the surface. The STM used the tunneling current from the substrate that is conducted to the metallic tip. On the other hand, the AFM has used theory of van der Waals force [22] to calculate the data from the tip and the surface by using the laser beam from the source shining on the cantilever with the tip and then receive the reflection

from the mirror to calculate the position by the position sensitive detector. After that, it has been processed to achieve the images as we desired (Figure 2.24). Now we used the AFM to characterize the samples. The purpose is to see the number and the density of the dots from topography, amplitude, and also the phase image with the non-contact mode, the oscillation from the tip at the resonance frequency. With the AFM capability, the images show below:

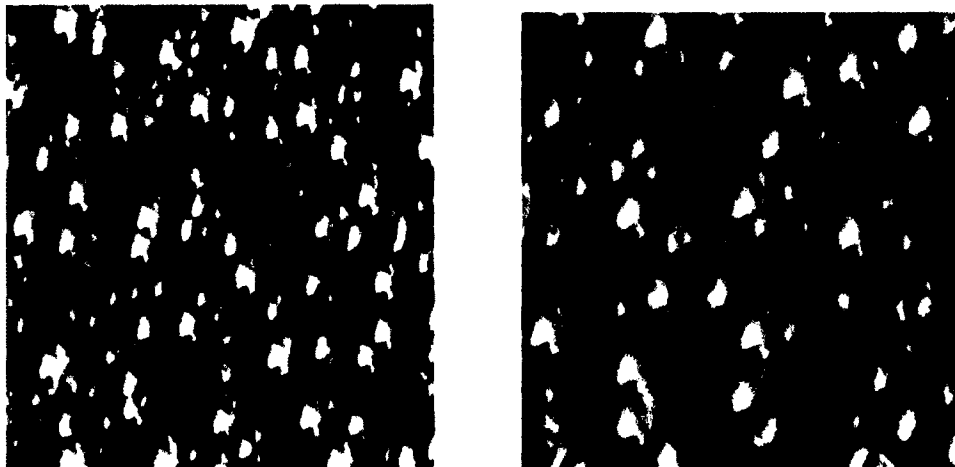


Figure 2.26a. AFM amplitude image (2 $\mu\text{m}$  $\times$ 2 $\mu\text{m}$ ) and 2.26b. The image size 1 $\mu\text{m}$  $\times$ 1 $\mu\text{m}$ .

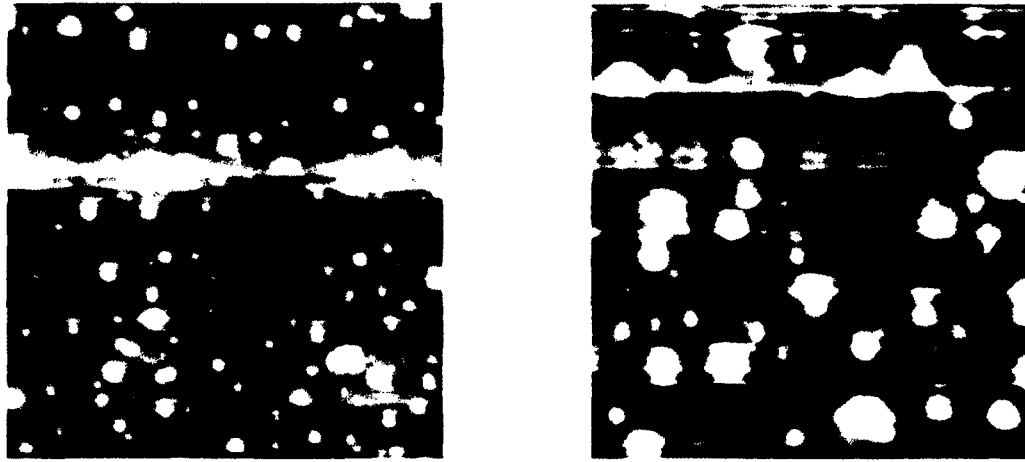


Figure 2.27a. Topography image ( $2\mu\text{m}\times 2\mu\text{m}$ ) and 2.27b. The image size  $1\mu\text{m}\times 1\mu\text{m}$ .

The advantage of AFM is to analyze the sample that we manufactured and to expect the possible results after finishing both the fabrication and the measurement. The next chapter is about the experiment and the results that will prove our research and the enhancement that we look for.

### **III. DARK CURRENT AND PHOTOCURRENT ANALYSIS**

#### **3.1 Dark Current Test Set up**

The dark current is one of the major noise that the researchers try to reduce as much as possible. In optical area, the dark current occurs when the light is absent from the source and the current will be in the device. It can be measured to see how much of the dark current affects the performance as I-V curve characteristic. The measurement set up in our research has used the foil to cover the chamber with 78 K temperature. The analytical formula is

$$J_{dark} = \frac{I_{dark}}{A}$$

{4}

J: The dark current density(A/cm<sup>2</sup>)

I : The dark current

A: The active area of mesa

With the test of the dark current, the following picture is the set up for testing the dark current at 78 K (Kelvin) with aluminum foil to prevent the light illuminating on the device in the chamber.



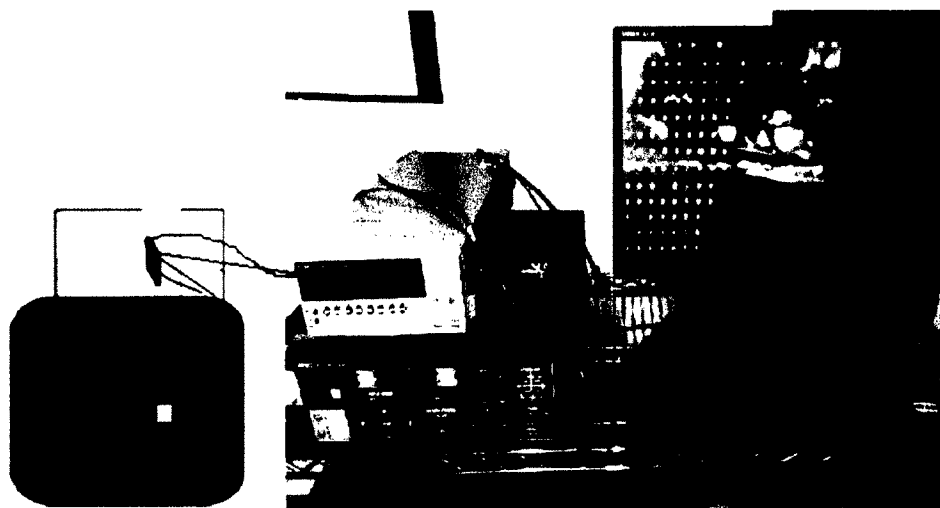


Figure 3.1 the setup of the dark current without aluminum shield [9].

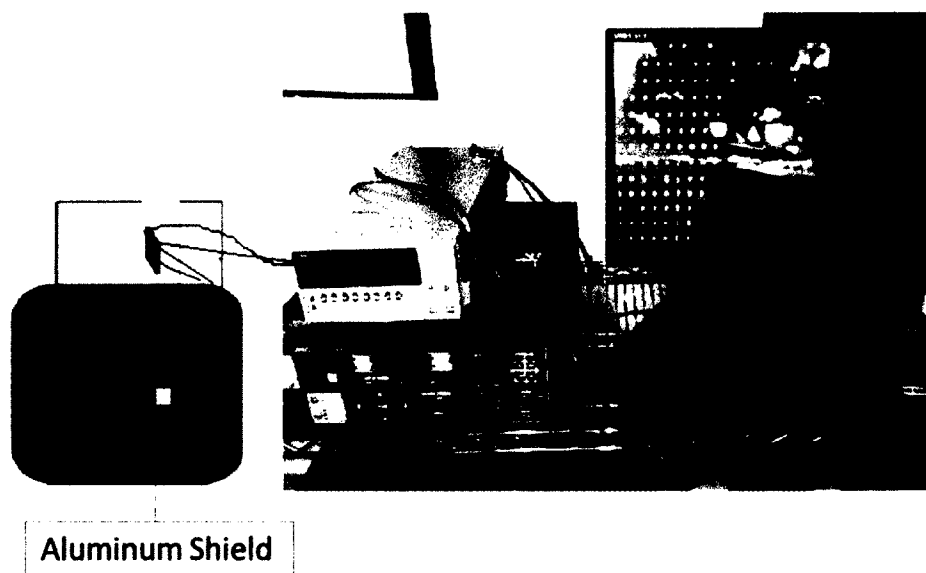
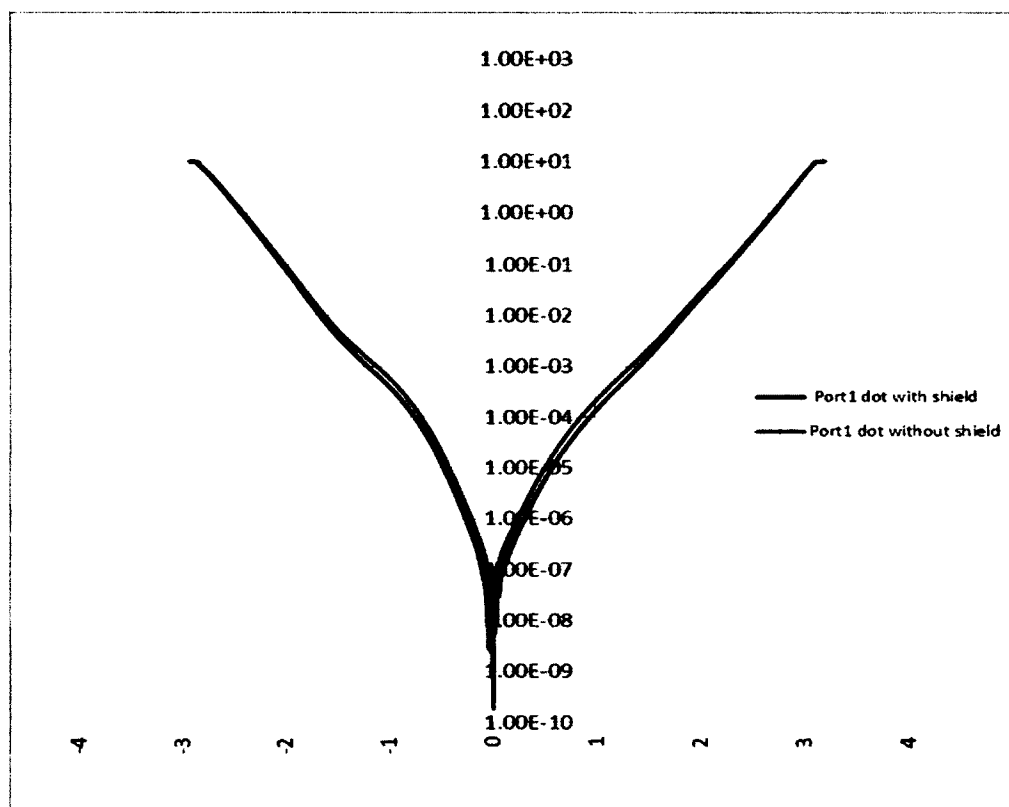


Figure 3.2 the setup of the dark current with aluminum shield [9].

### 3.2 The Dark Current's Experimental Results

In our research, the dark current has been measured in two conditions. First, the sample which is covered by aluminum shield has been tested into the chamber at 78 K. Second, the sample is tested for the second time within the chamber at 78 K without aluminum shield. After that, two outcomes will be compared to each other for analyzing the dark current affecting the performance of two structures (SP and Reference).

According to the figure 3.3 for the mesa1, the dark current density of mesa1 which is covered by the shield is less than the red curve which is a dot array testing without shield.



current to decrease the noise that radiate through the sample. In the meantime, even though the hole arrays enhancement is better than the regular structure, it still less enhanced than the dot arrays (Figure 3.6).

In the next result, we state the photocurrent that have affected the sample in many angles and how each angles have influenced through the plasmonic structure.

### **3.3 Photocurrent Test Set Up**

The photocurrent is significant for photodetector to drive the electrical signal from the electromagnetic wave. Generally, the photocurrent of quantum dot infrared photodetector is much better than the quantum well infrared photodetector. In our research, we tried to test and analyze the photocurrent between the normal structure of QDIP and SP of QDIP.

The black body (SBIR, Santa Barbara Infrared INC.) is the major source to radiate the spectrum and increase the temperature above absolute zero with the chopper that shuffles the frequency at 600 Hz in order to avoid the  $1/f$  noise through the samples inside the chamber. Then, the signal will be amplified at pre-amplifier and transit to the spectrum analyzer. (Stanford research systems, model SR760 FFT spectrum analyzer) with the same frequency at chopper.

Figure 3.3 the dark current density for Dot arrays at port 1(mesa1) with and without aluminum shield.

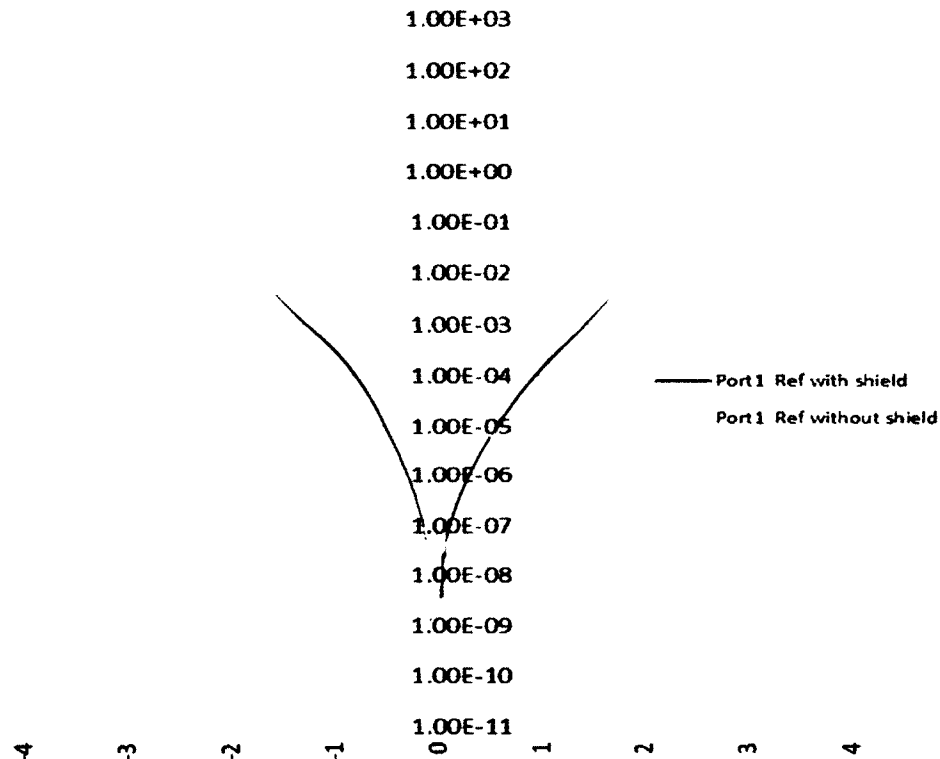


Figure 3.4 the dark current density for reference at port 1(mesa1) with and without aluminum shield.

The Ref (Regular Structure) has been measured with and without shield. Both of them have not fluctuated much when testing at the same condition as the dot arrays. Therefore, the background noise has influenced the dot arrays when testing without shield but it doesn't affect the ordinary structure. In addition, the plasmonic

structure is sensitive to block the background noise and the noise which is from the dark current without potential bias voltage input when testing with shield.

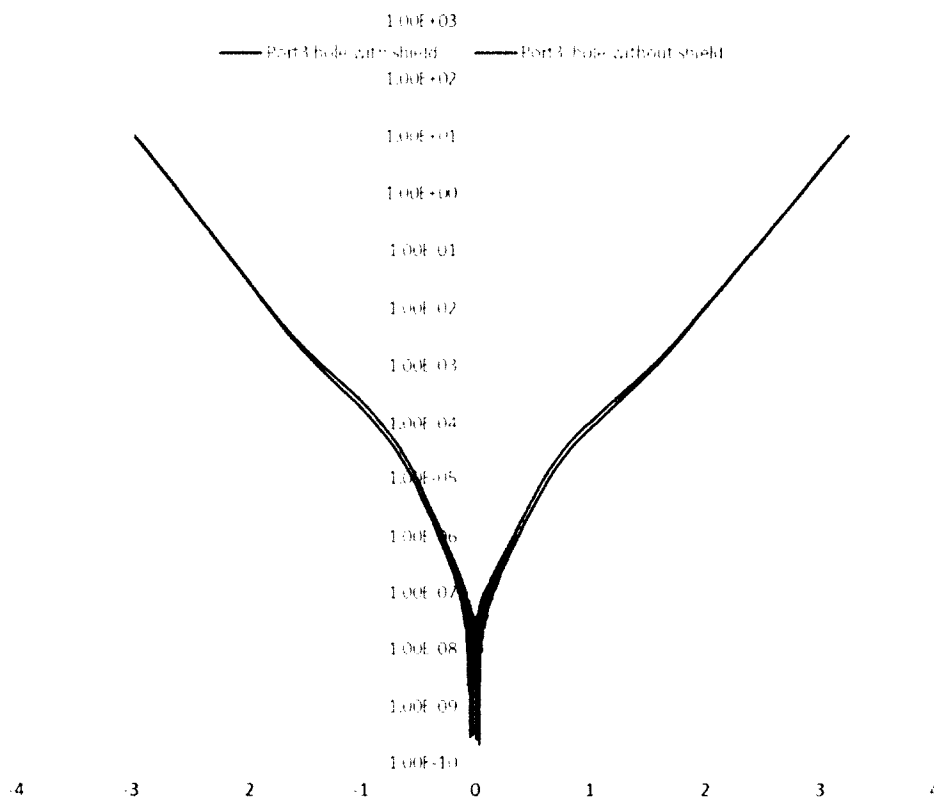


Figure 3.5 the dark current density for hole arrays at port 1(mesa1) with and without aluminum shield.

Based on the graph 3.5, we found the results of the dark current are similar to the dot arrays structure. The hole arrays with shield has lower dark current than the hole arrays without shield since the shield is in charge of blocking the background noise that radiated from both two sides of the sample. Hence, the dark

currents of both dot and hole arrays are decreased and lower than testing without shield as in figure below.

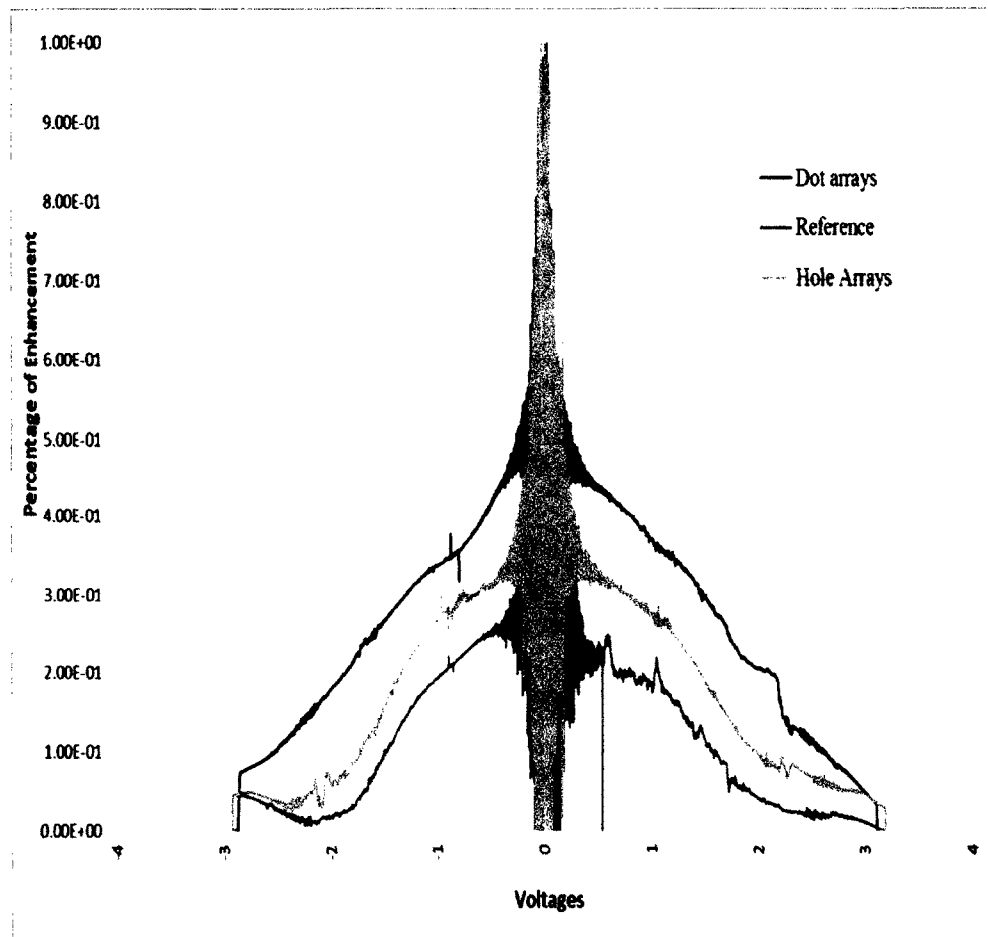


Figure 3.6 Percentage of Dark Current Enhancement.

For the graph above, the y-axis is the percentage of dark current enhancement between 0 and 1 and the x-axis is the voltages from -4 to 4. The blue line is the curve of the dot arrays, green curve for the hole arrays, and the red curve standing for reference (regular sample). We can conclude that the plasmonic structure affects the dark current. Such dot arrays have the strongest influence over the dark

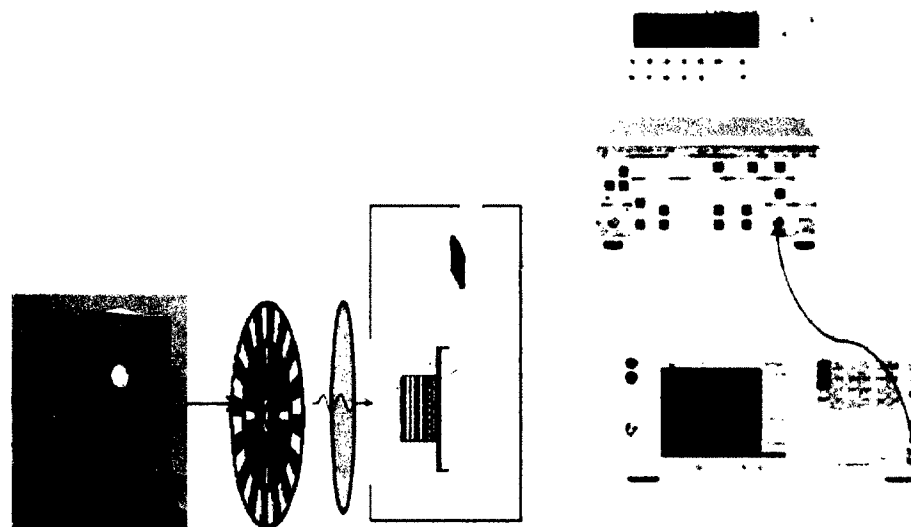


Figure 3.7 the photocurrent measurement without aluminum shield [9].

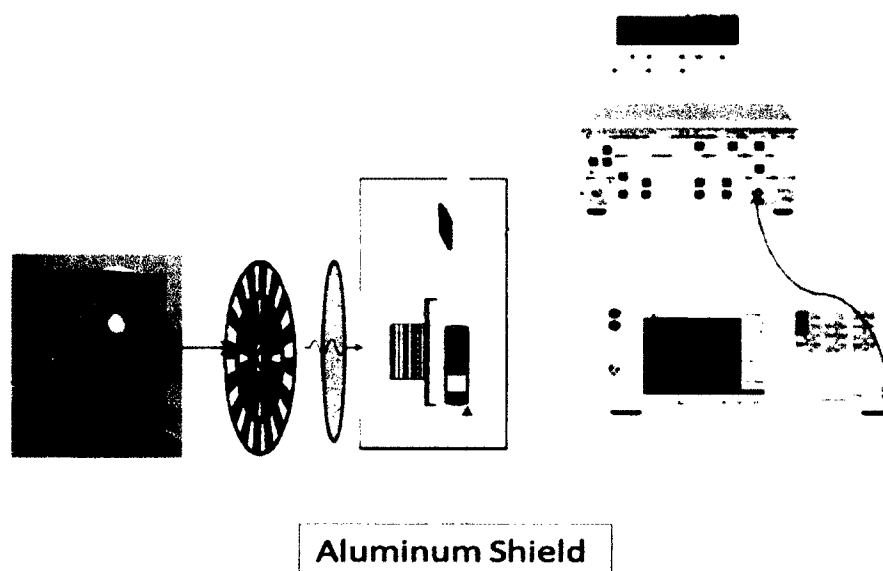


Figure 3.8 the photocurrent measurement with aluminum shield [9].

In this thesis, we test the photocurrent with and without shield at the different angles. The angles start from 0, 30, 45, and 60 to analyze the photocurrent when the black body shines on the sample into the chamber at 78 K. The bias voltage to apply for the pre-amplifier is the same as the noise current so that we would like to see the difference through the regular and plasmonic structure. In the next chapter, it is about the photocurrent's experimental results and analysis.

### **3.4 The Photocurrent's Experimental Results**

With the measurement of the photocurrent, the black body source plays the important role of the appropriate energy allowed to the device. The free electrons rise up on the barrier of the conduction band while applying the bias voltage and then gives rise to the photocurrent.

In this research, we test the sample with aluminum shield which is on duty to prevent the noise that is coming from both sides of the sample and we turn the sample in the different angles by starting from 0, 30, 45, 60 degrees. Therefore, the light source from the black body is permanently in the front of the sample while turning the sample in that angles. Furthermore, the light is confined only the hole of the shield and shining on the sample within the chamber at 78 K.



### 3.7 The measurement at different angles

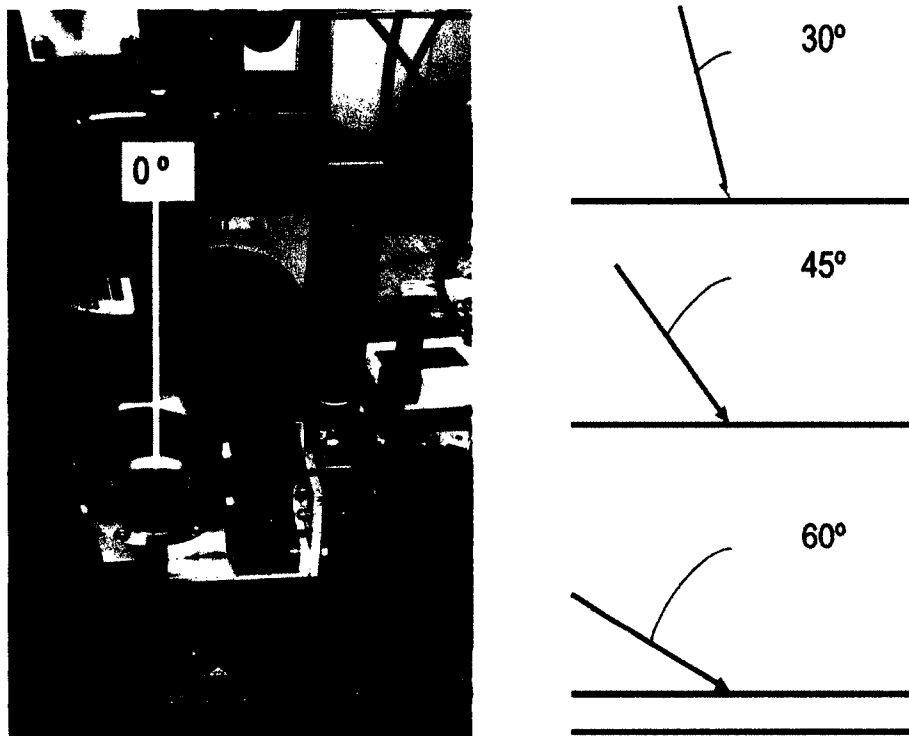


Figure 3.9 the angles test for the photocurrent.

### Measurement at 0 degree

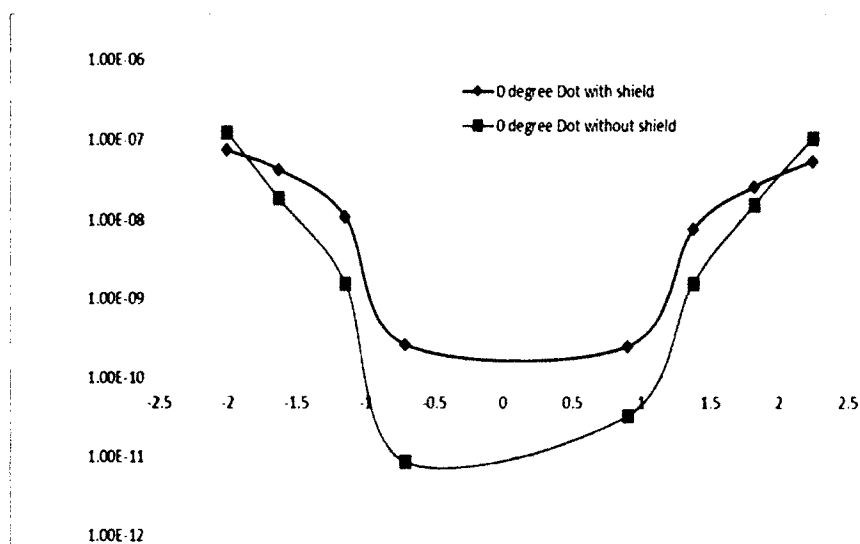


Figure3.10

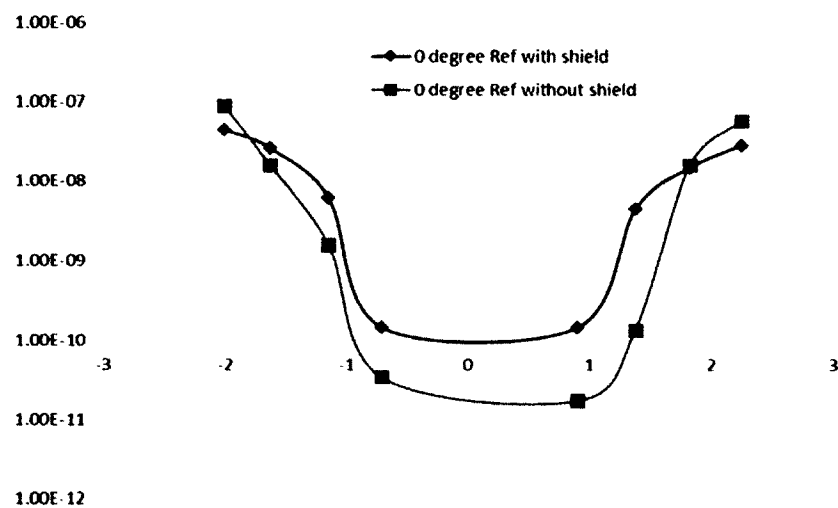


Figure3.11

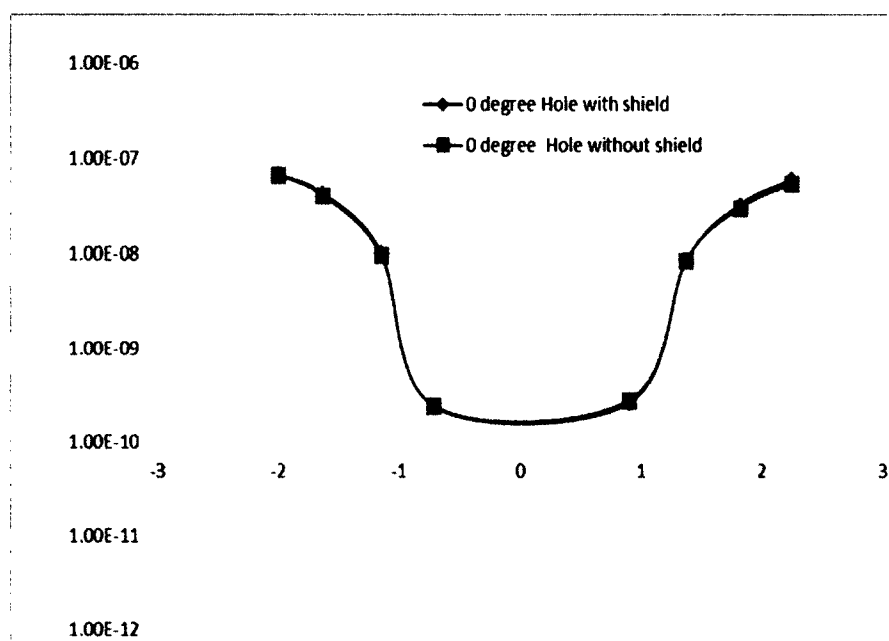


Figure3.12

### Measurement at 30 degree

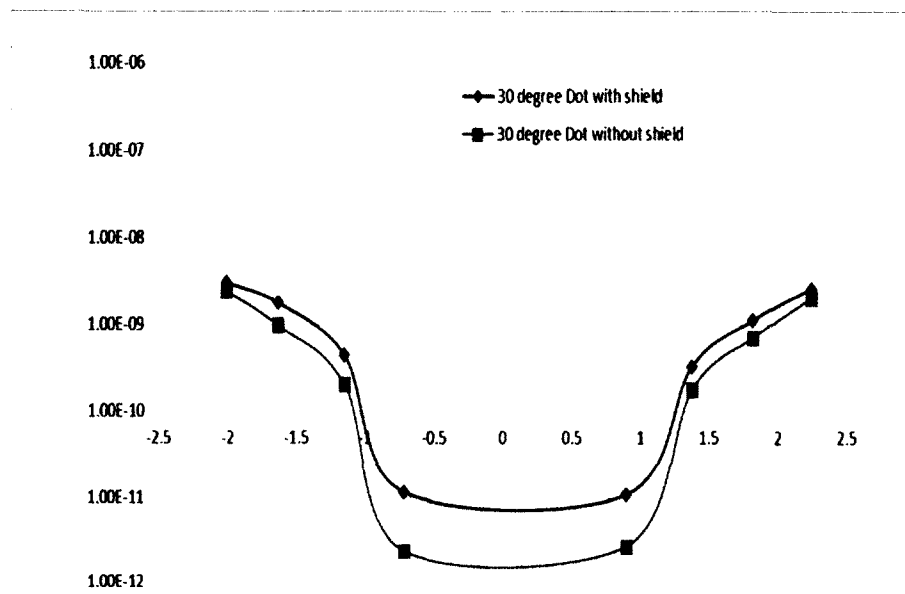


Figure3.13

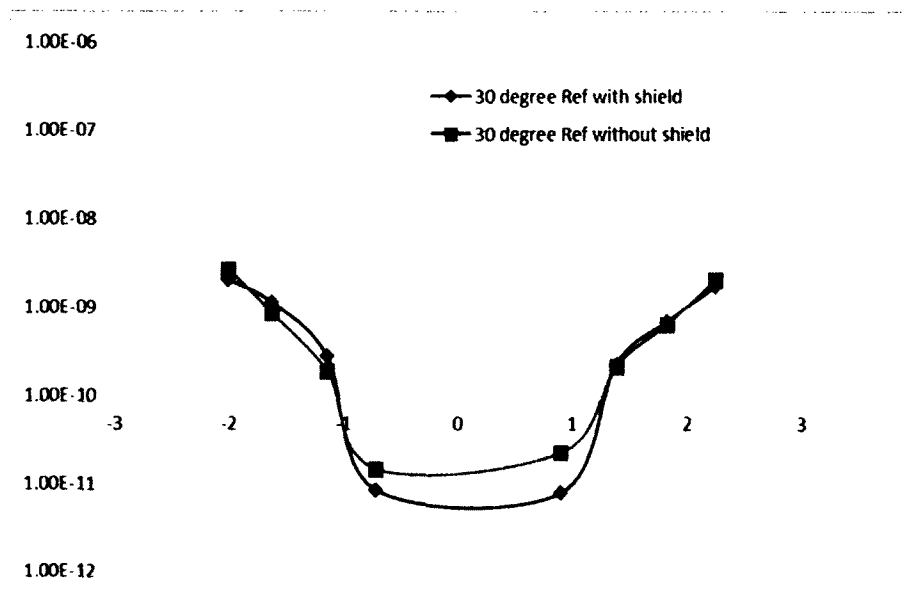


Figure3.14

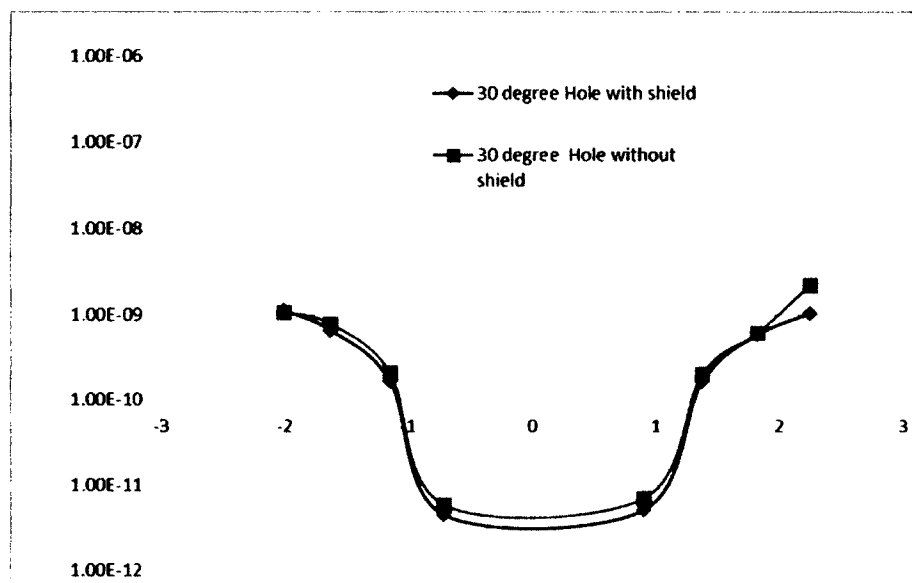


Figure3.15

### Measurement at 45 degree

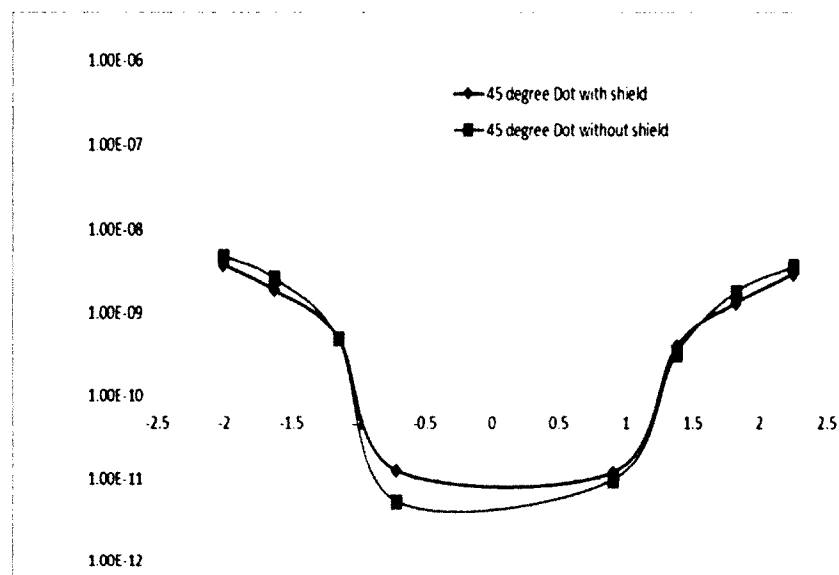


Figure3.16

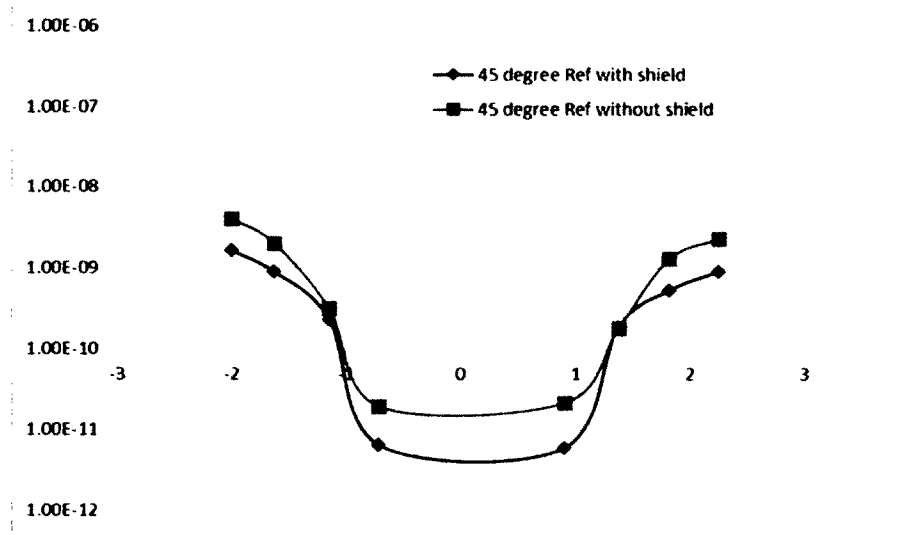


Figure3.17

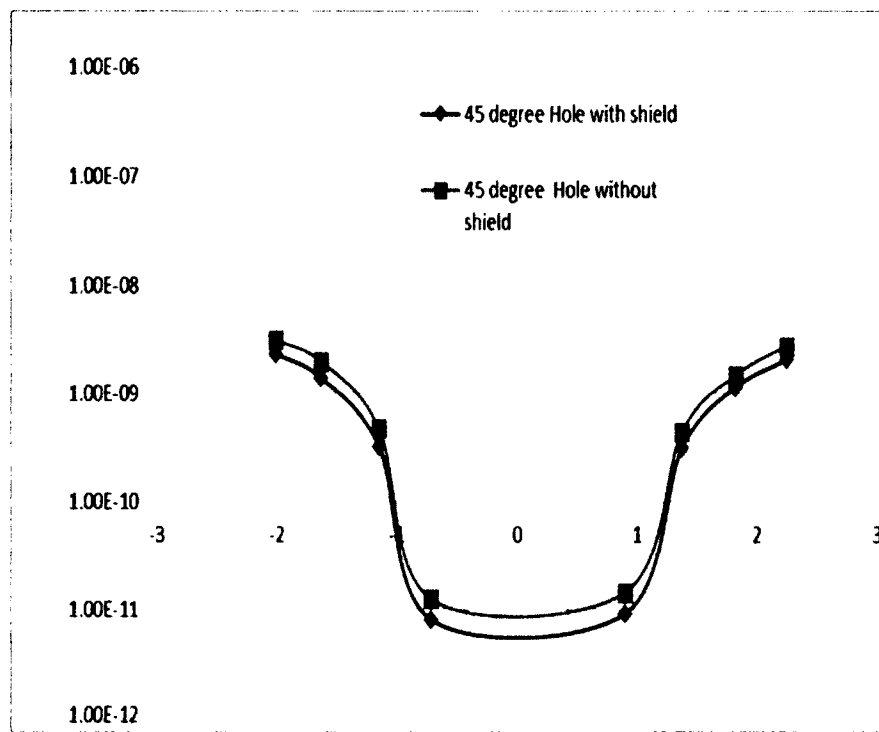


Figure3.18

### Measurement at 60 degree

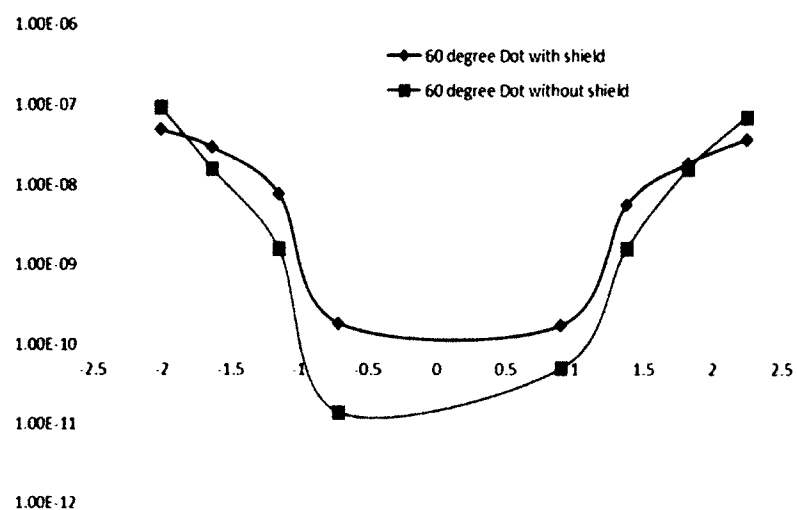


Figure3.19

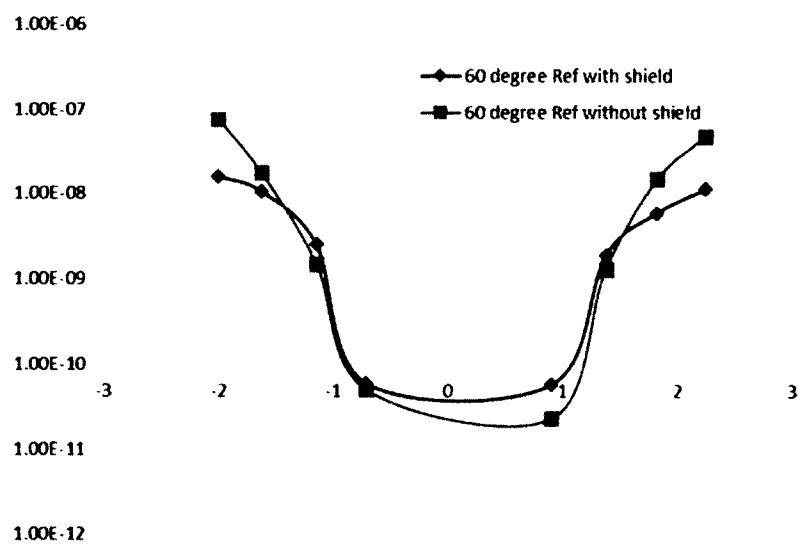


Figure3.20



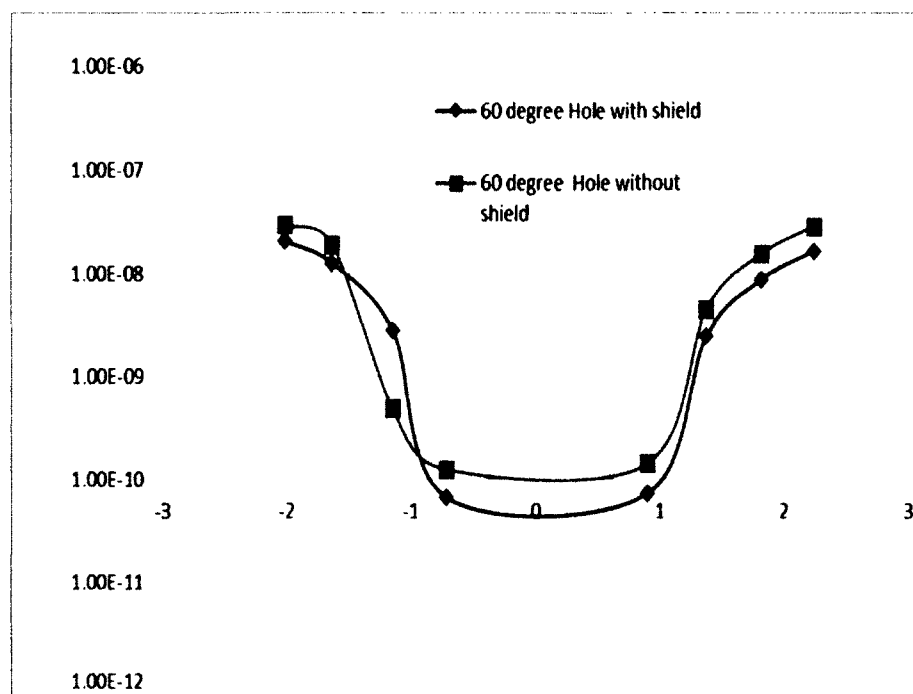


Figure3.21

According to the photocurrent of 0 degree (Figure9, 10, and 11) for dot arrays and regular pattern, blocking the background noise, it makes the photocurrent better than testing without shield. However, the hole arrays are different. The photocurrent of them doesn't change with or with shield. Therefore, the experiment has been keeping in the different angles, 30, 45, and 60 degrees from the black body source.

At 30 (Figure 12,13, and 14) and 45 degrees (Figure 15,16, and 17) the dot arrays have the photocurrent with shield that still is more than without the shield but the Ref( Regular structure) with shield is less than without shield. Also the photocurrent of hole arrays without shield is more than the measurement with shield.

At 60 degree of the photocurrent ratio (Figure 18,19, and 20), the dot arrays are constantly better than without shield and the Ref with blocking the noise by shield is back to has the photocurrent more than without shield. On the other hand, we found the photocurrent of hole arrays with shield is still lower than without shield from the photocurrent at 30, 45, and 60 degrees.

#### **The Photocurrent at different angles**

<b>Patterns/Angles</b>	<b>0 degree</b>	<b>30 degree</b>	<b>45 degree</b>	<b>60degree</b>
<b>Dot arrays</b>	Shield > W/o Shield	Shield > W/o Shield	Shield > W/o Shield	Still shield > W/o Shield
<b>Reference</b>	Shield > W/o Shield	Shield < W/o Shield	Shield < W/o Shield	Shield > W/o Shield
<b>Hole arrays</b>	Shield $\approx$ W/o Shield	Shield < W/o Shield	Shield < W/o Shield	Shield still < W/o Shield

Table1.1 the photocurrent at different angles.

Due to several measurements, the photocurrents in the different angles have different results. Therefore, we use the data as the photocurrent of dot and hole arrays and reference which are tested without shield to analyze the characteristics of nano-antenna by taking the ratio of the dot arrays over the reference in the different angles and also the ratio of the hole arrays over the reference (all of the samples have been measured only without shield condition). The results illustrate below.

at 0 degree	at 30 degree	at 45 degree	at 60 degree
dot/ref	dot/ref	dot/ref	dot/ref
1.835583247	0.993110236	1.55	1.460008288
1	1.079506934	1.363427697	1.070773793
11.52830189	0.811049724	1.775402248	1.211931645
1.897518014	0.120353982	0.456734317	2.177892919
0.249275362	0.162832101	0.279335304	0.277685624
1	1.069394642	1.566793893	1.053448276
1.189223215	1.112251882	1.272102161	0.897311342
1.379234005	0.889462049	1.151589242	1.226890756

Table 1.2 the photocurrent of the dot arrays over reference in different angles.

Table 1.2 illustrates the maximum values in the 0 degree. That means the radiation especially zero degrees is the biggest ratio or most powerful of the radiation comparing other angles, 45, 60, and 30 degrees respectively. Therefore, we can

strongly conclude that the dot array's structure is capable of the nano-antenna on the photodetector within the different angles.

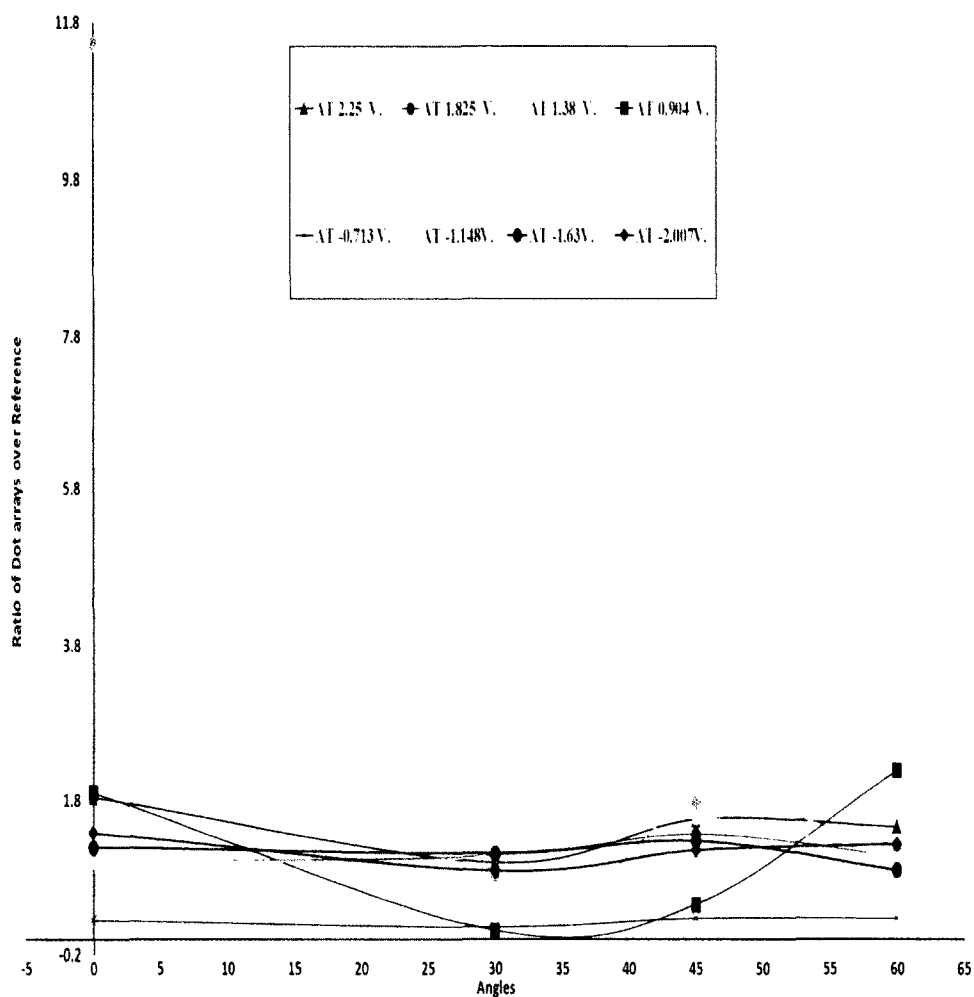


Figure3.22 the ratio of the dot arrays over the reference.

From the Figure 3.22, the photocurrent ratio of dot array without shield over references has been discussed that the magnitude of dot arrays at the 0 degree

has more power than others in 30, 45, and 60 degrees. Especially, with 30 degree the photocurrent ratio is the lowest. As we know that one of special ability of the plasmonic structure is collecting the electromagnetic field, the graph of the dot arrays over the reference brings about the radiation of antenna in the different angles.

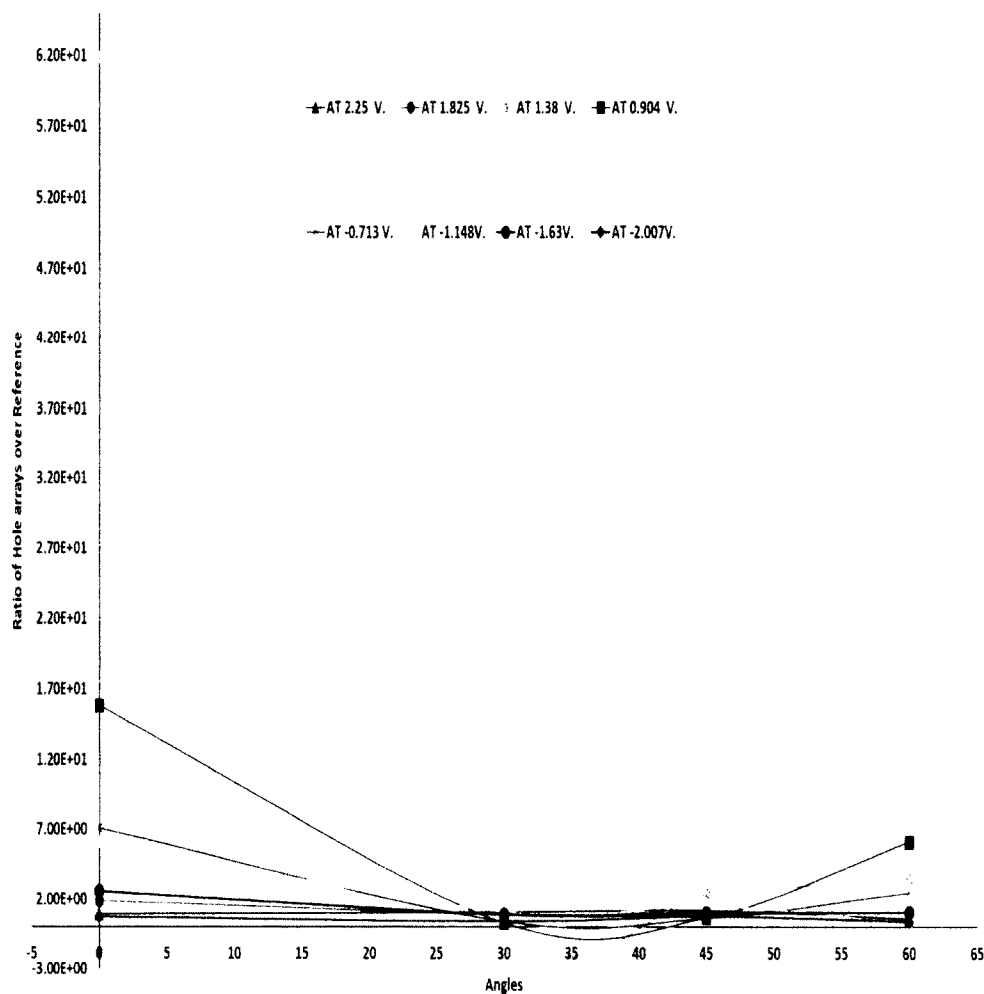


Figure3.23 the ratio of the hole arrays over the references.

0.949809623	1.094488189	1.21754386	0.5946954
1.906080826	0.94761171	1.132211171	1.046104071
61.84325109	0.925414365	2.457571082	3.443698505
15.80693126	0.312212389	0.66300738	6.111398964
7.084057971	0.404957546	0.638189418	2.476303318
6.104746318	1.097869648	1.534351145	0.327453581
2.577111922	0.902578143	0.966502947	1.093086308
0.755811379	0.400589536	0.767237164	0.387867647

Table 1.3 the photocurrent of the hole arrays over reference in different angles.

According to the Figure 3.23, the magnitudes of the hole arrays without shield are different from the dot arrays over the references. Half of the points in the 45 degree are less than and more than the points in 60 degree. That can be explained that the hole arrays has the characteristics in the antenna that slightly differ from the dot arrays while at 0 degree the values are still the biggest. Besides, at the 30 degree, the photocurrent ratio is still the lowest comparing with other angles similarly to the dot array's structure from the data in table 1.3.

#### **IV. CONCLUSION**

To summarize this research, the plasmonic structure is essential for quantum dot infrared photodetector device to decrease the noise from the radiation of background noise such as the radiation from the black body or any of materials around the device. For the dark current measurement with the aluminum shield to block the noise from the sides of the sample and without shield, the dot arrays, hole arrays, and the sample without plasmonic (Reference) on top are tested at temperature 78 K. The results of them are different from each other. The dot arrays with shield and the hole arrays with shield: both of them are less than the dot and the hole arrays testing without shield. On a contrary, the regular sample without plasmonic structure, after testing with and without shield, the dark currents are the same whether using shield or not. Further, the shield has the duty to block the noise from the sides of the sample. That means the noise is only coming from the front of the sample and affect the dark current. Therefore, according to the experiment of the dark current that we found and plotted, they explain and conclude the structures of dot and hole arrays can protect the noise that shining on the front of the sample and with the plasmonic feature such the dot arrays on the top of the sample is able to make the lowest dark current comparing with hole arrays, and reference respectively.

Based on the photocurrent measurement between the surface plasmon and the normal device at several angles, the photocurrent in the different angles has the different pattern of antenna radiation. From the photocurrent experiment, the structure of the dot arrays and hole arrays have ability of nano- antenna because the majorities

Hence, we can conclude the photocurrent in the different angles have the characteristic of the nano-antenna pattern like the circular aperture as the picture below.

### Three-dimensional field pattern of a constant field circular aperture

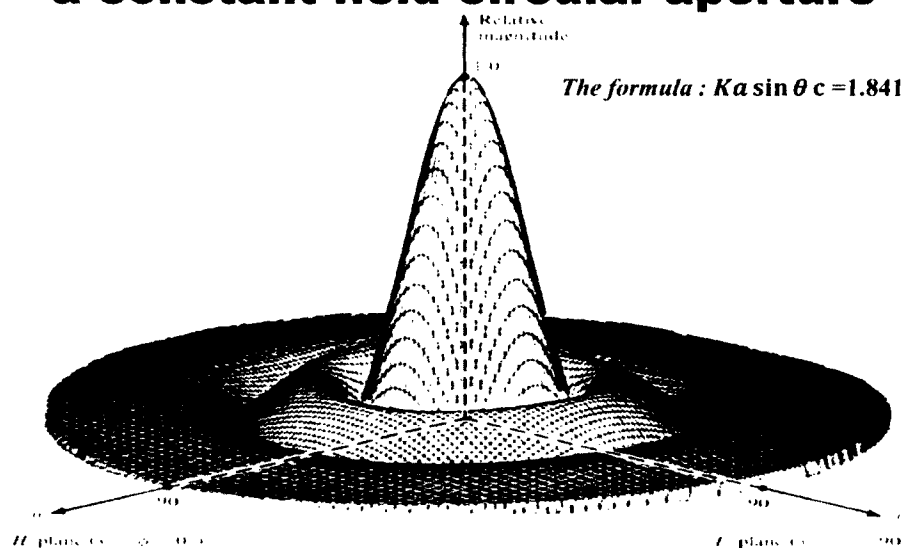


Figure 3.24 the three- dimensional field of the circular aperture.

*\*Image from Constantine A. Balanis, Antenna Theory, 2010*

In the next chapter, it is the conclusion that will brief the contents of the experiment and the results. They are related to each other in the dark current and photocurrent. In addition, we are able to sum up the performance of plasmonic structure and gives rise to future work.



of photocurrent values in 0 degree is the largest, 45, 60, and 30 degrees respectively. Especially, at the 30 degree the photocurrent ratio is the lowest comparing with other angles. However, the photocurrents of the hole arrays differ from the dot arrays especially in 45 and 60 degrees but they tend to go down when turning the sample to the 60 degree. In addition we also prove from the formula of the maximum other angles ( $Ka \sin(\theta) = 1.841$ ): after testing the maximum other angle is 45 degree, it is different from the ideal formula. For instance, the ideal formula giving the 30 degree is the maximum other angle. It can be explained that at 30 degree is uniformity and it is not able to have the side lobe as the pattern of circular aperture.

Hence, we are able to sum up that at the 30 degree whether dot or hole arrays have the lowest the photocurrent ratio when comparing with other angles and also at 0 degree, the photocurrent is the highest. That is result of most incidents that affect the photocurrent at the different angles and lead to the characteristic of the nano-antenna with the circular pattern which is the reference and related to the photocurrent as we did the measurement.

## **V. FUTURE WORK**

With the results due to the measurement, the structure of the dot and the hole arrays have obviously different results. Firstly, the constancy of the dark current in the hole and dot structure does not fluctuate by aluminum shield. Secondly, the special photocurrent in the different angles brings about the radiation pattern of antenna. Thus, the future work will emphasis the simulation of the radiation for the nano-antenna. From the following ratio tables we are able to use the data to analysis and do the simulation to support the possible results as we estimated.

at 0 degree	at 30 degree	at 45 degree	at 60 degree
dot/ref	dot/ref	dot/ref	dot/ref
1.835583247	0.993110236	1.55	1.460008288
1	1.079506934	1.363427697	1.070773793
11.52830189	0.811049724	1.775402248	1.211931645
1.897518014	0.120353982	0.456734317	2.177892919
0.249275362	0.162832101	0.279335304	0.277685624
1	1.069394642	1.566793893	1.053448276
1.189223215	1.112251882	1.272102161	0.897311342
1.379234005	0.889462049	1.151589242	1.226890756

0.949809623	1.094488189	1.21754386	0.5946954
1.906080826	0.94761171	1.132211171	1.046104071
61.84325109	0.925414365	2.457571082	3.443698505
15.80693126	0.312212389	0.66300738	6.111398964
7.084057971	0.404957546	0.638189418	2.476303318
6.104746318	1.097869648	1.534351145	0.327453581
2.577111922	0.902578143	0.966502947	1.093086308
0.755811379	0.400589536	0.767237164	0.387867647

Table of the photocurrent ratios of dot and hole arrays over the regular structure.

## **VI. LITERATURE CITED**

- [1] Fleck, Thilo Pierre Karl, Schubert, Stephan, Redlin, Matthias, Stiller, Brigitte, Ewert, Peter, Berger, Felix, & Nagdyman, Nicole. (n.d.), *“Influence of external cardiac pacing on cerebral oxygenation measured by near infrared spectroscopy in children after cardiac surgery”*, Pediatric Anesthesia, 2010.
- [2] Hudson, R.D., Jr. Hudson, J.W. *“The military applications of remote sensing by infrared”* Proceedings of the IEEE Year: 1975, Volume: 63, Issue: 1, Pages: 104 – 128.
- [3] Fabio Durante P. Alves, G. Karunasiri, N. Hanson, M. Byloos, H.C. Liu, A. Bezinger, M. Buchanan, *“NIR, MWIR and LWIR quantum well infrared photodetector using interband and intersubband transitions”*, Infrared Physics & Technology, Volume 50, Issues 2–3, Pages 182–186, April 2007.
- [4] Singh, Jasprit. *Semiconductor Devices: Basic Principles*. New York: Wiley, 2000.
- [5] Rostami A, Ravanbaksh N, Golmohammadi S, Abedi K. *“High-responsivity AlGaIn-GaN multi-quantum well UV photodetector”*. International Journal of Numerical Modelling, March 2014.
- [6] H.C. LIU., *“Quantum dot infrared photodetector”*, Institute for Microstructural Science, National Research Council, Opto-electronics review, Ottawa KIA OR6, Canada, 2003.

[7] P. NORTON, “*HgCdTe Infrared Detector*”, Santa Barbara Research Center, Raytheon Systems Company, OPTO-ELECTRONICS REVIEW 10(3), 159–174 (2002).

[8] Guiru. Gu, *BACKSIDE-CONFIGURED PLASMONIC STRUCTURE FOR QUANTUM DOT INFRARED PHOTODETECTOR ENHANCEMENT*. 2013, University of Massachusetts Lowell: United States -- Massachusetts. p. 37.

[9] PUMINUN VASINAJINDAKAW, *VERIFICATION AND REDUCTION OF DARK CURRENT ON QUANTUM DOT INFRARED PHOTODETECTOR*. 2009, University of Massachusetts Lowell.

[10] Ian Freestone, *Lycurgus Cup- a Roman Technology*, Cardiff School of History and Archaeology, Cardiff CF10, 3EU, Wales, UK.

[11] Ritchie, R.H., *Plasma Losses by Fast Electrons in Thin Films*. Physical Review, 1957. 106(5): p. 874-881.

[12] M.A. Noginov and G. Zhu, *Surface plasmon and gain media*, Nanophotonics and Surface Plasmon Book, p.144.

[13] Bohren, C.F. and D.R. Huffman, *Absorption and Scattering of Light by Small Particles*. 1983, New York: Wiley.

[14] Raether, H., *Surface Plasmons on Smooth and Rough Surfaces and on Gratings*. 1988: Springer, Berlin.

[15] Maier, S.A. *Plasmonics fundamentals and applications*. 2007

[16] Joachim Loos, *Art of STM Scanning Probe Microscopes in Materials Sciences*, Advanced Material, 2005, Volume 17, Issue 15.

- [17] J. Hao, J. Wang, X. Liu, W. J. Padilla, L. Zhou, and M. Qiu, "*High performance optical absorber based on a plasmonic metamaterial*", *Applied Physics Letters*, vol. 96, no. 25, June 2010.
- [18] Govind Dayal and S. Anantha Ramakrishna, "*Design of highly absorbing metamaterials for Infrared frequencies*," *Opt. Express* 20, 17503-17508 (2012).
- [19] M. Diem, T. Koschny, and C. M. Soukoulis "Wide-angle perfect absorber/thermal emitter in the terahertz regime", *Physical Review B*, vol. 79, no. 3, Jan. 2009.
- [20] C. Cheng, M. Abbas, C. Chiu, K. Lai, M. Shih, and Y. Chang, "Wide-angle polarization independent infrared broadband absorbers based on metallic multisized disk arrays", *Optics Express*, vol. 20, no. 9, pp.10376-10381, April 2012.
- [21] Katherine A. Willets and Richard P. Van Duyne, "Localized Surface Plasmon Resonance Spectroscopy and Sensing", *Annual Review of Physical Chemistry* Vol. 58: 267-297, May 2007.
- [22] Hans-Jürgen Butt, "Measuring electrostatic, van der Waals, and hydration forces in electrolyte solutions with an atomic force microscope", *Biophys J.* 1991 Dec.
- [23] Constantine A. Balanis, "*Antenna Theory*", Third edition, 2010.







